

Forschungszentrum Karlsruhe
Technik und Umwelt

Wissenschaftliche Berichte
FZKA 6013

Determination of the Crack Pattern of Quenched Zircaloy Tubes

L. Steinbock

J. Stuckert

Institut für Materialforschung I
Projekt Nukleare Sicherheitsforschung

Forschungszentrum Karlsruhe GmbH, Karlsruhe

1997

Summary

The quenching of LWR cladding is investigated in order to understand the behaviour of a LWR core during the injection of water in the course of a possible accident. A series of single tube tests is conducted in order to establish a data base providing information about the phenomena: oxide layer formation, cracking and hydrogen generation. Oxide layer formation and cracking after the experiments may be documented with a microscope and an image processing system.

The hardware, the preparation methods and the software of this tube surface documentation system are described in the report.

A number of tube surfaces have been examined. The class of penetrating cracks was found to be correlated with the oxide layer thickness. The density of these cracks was traced with programmed algorithms and by hand. The hand-generated crack nets are considered to be more realistic because interference from surface stains and different crack width are avoided by the human examiner.

Bestimmung der Rißstrukturen von abgeschreckten Zirkaloyrohren

Zusammenfassung

Das Abschrecken der Hüllrohre eines Leichtwasserreaktors wird untersucht, um das Verhalten des Reaktorkernes während des Wasserflutens nach einem möglichen Unfall zu verstehen. Eine Reihe von Einzelrohrversuchen wurde durchgeführt, um Informationen über die Phänomene Oxidschichtwachstum, Riß- und Wasserstofferzeugung zu erhalten. Die Oxidschichtdicke und die Risse können mit einem Mikroskop und einem Bildverarbeitungssystem dokumentiert werden. Die instrumentelle Ausrüstung, die Präparationsmethoden und die Rechenmethoden werden hier beschrieben.

Eine Anzahl von Rohroberflächen wurde untersucht. Die Klasse der durchgehenden Risse korreliert mit der Oxidschichtdicke. Die Rißdichte wurde mit Programmen und mit Hand bestimmt. Die handbestimmten Rißnetze wurden als realistischer angesehen, weil der Einfluß von oberflächlichen Flecken und von unterschiedlichen Rißbreiten durch den Untersucher vermieden wird.

Contents

- 1. Introduction.....3
- 2. Image Capture System.....3
- 3. Crack Visualization Method.....3
- 4. Illumination Correction.....4
- 5. Image Assembling Methods.....4
- 6. Image Analysis Methods.....5
- 7. Evaluation of Pin Surfaces.....6
- 8. Crack Density Comparison.....9
- 9. Conclusions.....9
- 10. Tables.....11
- 11. Appendix.....12
- 12. Figures.....16

1. Introduction

When partially oxidized Zircaloy fuel rod cladding tubes are quenched from high temperatures by water or steam cracks develop in the oxide layer and the brittle α -Zr(O). The cracks are formed by stresses generated in the clad materials by differential thermal expansion of the various layers on cool down. In order to understand and describe the physico-chemical behaviour of the Zircaloy cladding by physical models an extensive data base is needed which will be provided by the quenching experiments performed at FZK. The geometrical form and the density of the cracks (crack length per unit area) in the oxide layer and partially in the metallic substrate have to be known. A high crack density increases the active surface for oxidation and hydrogen generation. In cases with thick oxide layers the new surfaces generated by cracks are the predominant sites for new oxidation and hydrogen generation.

Different methods are available for the detection of cracks. Radiographic imaging shows even small cracks in tubes without ZrO₂ pellets but the high absorption of the pellets leaves too few photons for generating good images with low noise.

Crack detection with ultrasound (US) is another widely used method. However the oxidized Zircaloy cladding wall has three layers of different elastic properties, is very brittle and has many cracks. Therefore the generation and interpretation of the US signals is very difficult.

Thus in a first attempt we tried to visualize the cracks with a stereo microscope and a video camera coupled to one branch of the optical paths.

In the following the methods for producing the images of the tube surface and for analyzing the cracks and their density are presented and discussed.

2. Image Capture System

The cracked Zircaloy tubes are mounted on a motorized table which allows axial and rotational positioning under the objective of a LEICA M10 stereomicroscope ([Fig. 1](#)). The position control system allows imaging of consecutive sections of a tube under constant illumination. The light may be polarized and color filtered. The image is digitized with a MegaVision T2 camera of high resolution (2048x2048 picture elements) and stored as a TIF-File. Positioning tables and camera are controlled by a Pentium PC and the image processing program OPTIMAS. Thus a series of contiguous images may be generated which cover a tube surface from top to bottom ([Fig. 2](#)) and around the circumference ([Fig. 3](#)).

3. Crack Visualization Method

Preliminary tests showed that a polarizing filter is necessary in order to suppress the glancing artefacts which are due to surface curvature of the tube and in order to reduce glare at small wrinkles generated by the drawing process of the tube. With polarized light white crack lines in the oxide layer appear, which are not visible without polarization. The open cracks in oxidized tubes with more than 300 μm oxide layer thickness are accompanied sometimes by laminar bands of white shining lines more or less parallel to the main crack line ([Fig. 4](#)). These laminar white bands are visible also at other sites without open cracks. When investigating the inner side of a tube we found cracks in the adjacent α -Zr(O) at the location of the laminar white bands ([Fig. 5](#)). In order to verify the hypothesis of the crack linkage to the laminar white bands we injected a liquid penetrant into the tube and watched what happened at the laminar bands. Most of them went darker and some of them showed bleeding of colored liquid diffusing out of the cracks ([Fig. 6](#)). However the red coloring changes the

reflectance after drying and the initial diffusion of the liquid overemphasizes locations where the crack width is wide and shows bleeding.

Nevertheless the penetration of the liquid solvents through the cracks shows that the laminar white bands are micro cracks not yet opened to the surface. A SEM image (Fig. 7) shows such a crack opening at the inside surface of the α -Zr(O) and some smaller cracks parallel with the main crack. At the outer surface the crack is almost closed.

The physical explanation of the reflectance (latin: albedo) decrease after wetting may be the following: the zirconium oxide is a semitransparent material with many small voids between the columnar grains. At the air-oxide interfaces light is scattered and reemerges to the surface. When liquid has filled the voids the amount of scattering at the liquid-oxide surface is smaller and the light penetrates deeper into the oxide and is absorbed at the oxide/ α -Zircaloy interface. Thus the albedo is lower in the neighbourhood of the cracks.

4. Illumination correction

The illumination and reflection of the surface is not uniform due to tube curvature and parallax change from center to the corners of the image. In order to generate the reflection of a white tube with the same diameter a white tape was glued on the surface of a new Zircaloy tube with 10.75 mm diameter and the image taken as reference illumination. An OPTIMAS macro hellnorm.mac was written which divides the raw image by the reference reflection image. After this normalization the grey value in the images indicate the albedo change in each point compared to the reference albedo (Fig. 8).

The correction of the varying pixel area due to curvature and parallax is not yet implemented but will be developed later. It will change the crack length by some percent only which is negligible in the context of the present errors induced by insufficient feature classification of the present OPTIMAS macros.

5. Image Assembling methods

In order to analyze a cracked surface of a Zircaloy tube with mathematical algorithms a single image like Fig. 4 is not sufficient to get a reliable result. It is necessary to make many images which cover the whole circumference and most of the hot length of the tube. However Figs. 2 and 3 show considerable changes in image illumination at the border between neighbouring images. This is caused by non uniform illumination of the field of view. Since the surface curvature changes the reflection intensity and the focus depth of the microscope deteriorates rapidly when leaving the horizontal center line, it is necessary to scan narrow subimages covering only a small circumferential angle and to assemble a mosaic image covering the whole circumference later.

The first pins were scanned manually, that means the rotation was done by hand with the pin lying in a linear race of ball bearings on each side. About 12 images covering each about 40 degrees were acquired. Afterwards an empty image was generated and the small subimages were assembled with COREL PhotoPaint under visual control. Subimages covering 360 degree images (2pi image in the following) with feature matching at the edges were generated in this manner. From pin 1906 such circumference images were acquired at 5 locations (Figs. 21 to 25).

Later the scanning was automated. The circumferential scanning angle was chosen to 40 degree. When analyzing the first circumferential series of images manually it was found that the overlap at corresponding edges is not a constant (Fig. 9). This is due to bending and deviations of the tube circumference from an ideal circle. An OPTIMAS macro (*collage.mac*

in Appendix A) was written in order to determine the lines at the edges of neighbouring images which are matching best. The best match was calculated by correlation. Having found the cutting lines in each subimage a contiguous 2pi image may be assembled showing the whole circumference. The spatial calibration is done with a regular millimeter grid glued on a Zircaloy tube with 10.75mm diameter.

6. Image Analysis Methods

After the surface of a pin is scanned and assembled it may be analyzed with the tools of an image processing program like OPTIMAS. This system provides a number of different mathematical algorithms (tools) in order to extract quantitative results from an image. There are several levels of sophistication in the tool hierarchy.

The **pointwise** operations change the value of a pixel independent from its neighbouring pixels. Three operations are important for us:

1. Additive or multiplicative correction of non-uniform illumination fields (already shown).
2. Histogram operations for pattern emphasis or poster generation (Fig. 10).
3. Spatial distortion correction for curvature and parallax errors.

Area filtering processes the picture elements together with their neighbourhood and is needed for several purposes (Fig. 11):

4. Average, median or gaussian filtering reduces random noise in the image.
5. Edge filters (x-and y-edge, Sobel) use convolution filtering for extracting edge lines.
6. Fourier filtering is the most general algorithm which allows to suppress unwanted and to enhance wanted features in an image.

A third group of algorithms derives new objects in the image.

7. Statistical analysis of the histogram provides parameters which are needed in order to enhance contrast.
8. Morphology analysis extracts sets of lines or areas from an image which are peculiar in some defined way and which represent physical objects like cracks or stains.
9. These sets may be analyzed by mathematical functions which extract further informations like length of cracks, perimeter or circularity of areas and so on.

All these operations may be commanded by clicking the associated icon of the tool. But OPTIMAS allows also to run these operations in a pre-defined way. For that purpose the user writes a macro: a block of lines with ALI (Analytical Language for Images) statements. In Appendix A some of the macros which have been written for the analysis of cracked tube surfaces are documented.

As an example the algorithms of the ridge filter „hellgrat.mac“ documented in Appendix A.2 are explained in the following: Gaussian averaging with 5 pixel width (Gaussian 5x5) smoothes out random noise, convolution with a set of filter coefficients emphasizes the x-ridge and y-ridge, the absolute value (squaring and adding) indicates a ridge in any direction. After these operations the ridges are much brighter than before. An offset is subtracted and the sum is normalized to keep the gray values inside (0,255). The threshold operator generates a binary image of the ridges which is then skeletonized. This means OPTIMAS generates new line objects representing the skeleton net. All line object classes are extracted from the set of skeleton lines. The object classes important for crack analysis are: number of crack lines, line length, line angle to reference line, line width, and average line luminance.

Several other macros may further classify the line and area objects. For instance noangle.mac discriminates all lines parallel or perpendicular to the tube axis (line angle between 0, 90, 180,

270 ±3 degree). „Minlang.mac“ discriminates all lines shorter than a pre-determined length. „Nocircle.mac“ eliminates areas which have circular form. The macro „craclang.mac“ was written for the crack density calculation after hand tracing.

7. Evaluation of pin surfaces

A number of pins with different crack patterns have been analyzed so far. The assembled images are discussed, the crack density is calculated with OPTIMAS macros and the crack patterns are traced by hand. The OPTIMAS generated crack densities are given in the following text. The hand traced crack densities are compared in Table 1. The experiment naming convention is ddmmy.n (d=day, m=month, y=year, n=number on that day). Since usually only one experiment was conducted per day the last digit is omitted when not necessary. The quench facility is described in the report FZKA 5864 and the data of the experiments are accessible with a FTP program under the address 141.52.128.149 with MS Windows-NT protocol, the User-ID „IBRAE“ and the password „quench“.

Experiment 10096

The pin 10096 (water quenched from 1400° C, 300 µm oxide layer thickness) was a first try to analyze the surface along the whole tube specimen length of 150 mm ([Fig.12](#)). At that time the circumferential stepping mechanism was not yet operational and the pin was scanned at one angle only. The axial step width was about 11 mm and 13 images were necessary to cover the whole length of the pin.

From bottom to top a series of different regions may be discerned. The lowest 20 mm are dark with no cracks or other changes in the surface appearance. Because this region did not attain high temperatures like the central parts of the pin it has maintained its original appearance. From 20 to 30 mm the albedo (reflectance) of the surface increases to very bright. The bright ring is very regular around the whole circumference of the pin. Further up the albedo drops within a very short distance and the first cracks appear. Between 30 and 60 mm axial and circumferential white line marks are predominant. These marks are small defects in the oxide layer and seem to be generated during the drawing process of the tube. Further up until the center thermocouple ring cracks associated with laminar white lines appear. Most of the cracks are closed and some are open. Some of the bands are associated with an albedo increase of the surface. From center to about 10 mm below the top of the pin the density of white laminar bands and the number of open cracks increases.

This qualitative surface description was also analyzed with some OPTIMAS-macros. The albedo macro calculated the average relative albedo of the surface ([Fig. 13](#)) as a function of the height. The albedo in the lower white ring is twice as high as the base albedo of the tube in the hot center region. The albedo probably is dependant on the thickness and structure of the ZrO₂ layer of the tube.

The open cracks were analyzed with the „darkgrat“ macro. [Fig. 14](#) shows some isolated peaks at the location of the visible black cracks. Each bar in the figure is a measure of the crack length within a 0.5 mm wide stripe of the subimage. The peaks in the lower white band are an artefact showing the limit of this algorithm.

The white laminar bands counted with „hellgrat“ macro ([Fig. 15](#)) show an irregular behaviour in the central region. The high density at the upper hot to cold interface is probably caused by the different temperature history compared to that at the lower interface.

Experiment 28056

In the experiment 28056 the tube was oxidized to about 350 μm and not cooled by steam or water but only by the ongoing argon flow. The tube showed some open cracks and many laminar white lines. It was very brittle and broke during positioning under the microscope. Most of the broken parts were glued and the pin was scanned from 4 different sides (Fig. 2). The pin was the first treated with the liquid penetrant (Fig. 9 and 16). The albedo decrease in the center of the laminar white bands is due to permanent red coloring. After the circumferential positioning went operational a series of 3 adjacent or overlapping circumference images was scanned and analyzed with the „acetone“ macro in order to calculate the crack length of the visible cracks (Fig. 17). The automatically generated crack images show the limits of automatic feature classification. The rather sharp open cracks are delineated by one line only, but the laminar bands of white cracks are represented by a tangled net. More sophisticated algorithms might be possible to reduce such tangled nets to a straight line representing the most probable underlying crack line. For the undergoing examination it was decided to rely more on hand tracing of the cracks. The calculation of the total length of the automatically generated crack lines yielded 295, 379 and 293 mm in each of the three circumference images. With an image area of about 450 mm^2 the crack density is of the order 0.66 to 0.85 mm/mm^2 .

Experiment 03037.1

The pin 03037.1 (steam cooldown from 1200° C, 200 μm oxide layer thickness) is from a series of tests with varying oxidation time and shows typical crack lines after wetting with acetone. Two sections of 14.8 mm length were scanned and assembled (Fig. 18 and 19). The images were treated with the macro „acetone.mac“. This macro generates a grid of lines indicating the zones where acetone has lowered the albedo of the surface. Crack lines with moderate production of acetone are represented well, but wide cracks with laminar white bands at the crack center are represented as double lines. The same is true for areas with lowered albedo caused by another modification of ZrO_2 . The crack lengths are 444 and 514 mm giving a crack density of about 1 and 1.1 /mm, respectively. Later the crack net was generated by hand tracing giving a total crack length of only 230 mm or about 0.46/mm.

Experiment 21027

This pin (steam cooldown 1200° C, 300/340 μm) was cut after the experiment. The most interesting part was scanned (Fig. 20) and the crack length analyzed. Because the acetone solvent generated very broad bands with lowered albedo most of the laminar bands are outlined by more than one or two lines. In the upper part of the image a dark modification of the ZrO_2 is visible inside the bright ZrO_2 areas. An attempt was made to suppress the contribution of these areas to crack lines by proper selection of the threshold for skeletonizing the crack areas. The analysis yielded 1118 mm of crack lines or about 2.5 /mm, whereas hand tracing yielded 0.31 to 0.57 /mm.

Experiment 19066

This pin was quenched with water at 1600° C and with an oxide thickness of 300 μm showed many different surface patterns along its length. Five typical circumference images will be discussed in the following. At the lower cold-hot interface (Fig. 21) from 22 to 37 mm the border between white and dark ZrO_2 is very sharp and there are many laminar crack lines. The albedo decreases with solvent injection and shows where these cracks are connected to a through crack. The first open circumferential crack is visible at 55 mm (Fig. 22). It is accompanied by many laminar lines. Further above between 92 and 106 mm there are very few open (black) and red laminar crack lines (Fig. 23). Another 20 mm above between 110

and 124 mm (Fig. 24) there are several circumferential cracks with associated laminar crack lines. The line-free regions seem to be unbroken plates. At the upper hot-cold interface between 128 and 145 mm a last circumferential crack is visible at the right side of the image (Fig. 25). Then further upward many white laminar crack bands appear and at the right border of the image some very bright ZrO₂ areas are visible. A calculation of the crack length was not done, since the solvent-filled image (Fig. 21) showed a big difference between the open cracks and the laminar white lines and because the variability of crack patterns along the height is considerable.

Experiment 05066

This pin was water quenched from 1400° C and had an oxide layer thickness of 300 µm. This pin was difficult to analyze because the filling with liquid penetrant showed different crack behaviour at 60 mm (Fig. 26) on opposite sides of the tube. On one side the red liquid produced broad colored areas around an otherwise invisible crack (top of the circumference image) and on the other side of the circumference normal red-colored thin crack lines were visible (bottom of the circumference image). It is obvious that analysis with an OPTIMAS macro would lead to doubtful results. Therefore a crack grid was generated manually using the computer mouse as the tracking instrument. The length of this grid is about 175 mm and the crack density is 0.36/mm.

Experiment 27027

This pin has an oxide thickness of 300 µm and steam cooldown was initiated at 1600° C. It was scanned at the location of the central thermocouple ring (Fig. 27). The traces of this ring generate some additional cracks during analysis with acetone.mac. The total crack length is 456 mm or about 1/mm. Since part of the cracks is due to the traces of the thermocouple ring, the crack density is better estimated to be 0.9/mm.

Experiment 08047

This pin has only two axial crack lines at opposite angles and a corresponding crack density of 0.07/mm. Because of the simple crack geometry no image was taken and no OPTIMAS analysis was done.

Experiment 09047.2

This pin has two main axial cracks at about 180° distance and many circumferential cracks which meet the axial cracks more or less orthogonally (Fig. 28). It was the first to be scanned over the whole hot length between 20 and 118 mm. The crack density varies between 0.3 and 0.7/mm from top to bottom.

Experiment 10047

This pin was scanned between 27 and 101 mm, but Fig. 29 shows only the part between 27 and 83 mm. The crack traces generated by the solvent are not stable in this case and dark stains not connected to cracks disturb the analysis with acetone.mac. Thus the crack pattern was generated by hand. The crack density increases from at the bottom 0.33 /mm to 0.57 /mm at the top.

Experiment 11047

This specimen showed dark and white patterns on the surface which resembled crack patterns (Fig. 30). The injection of solvent however showed no penetrating cracks. An examination with an eddy current probe indicated that the dark areas have an oxide thickness of about 180 µm and the white areas of 200-220 µm.

Experiment 20027.2

This tube was scanned between 70 and 112 mm (Fig. 31) and shows a dense crack pattern in the hot central region where the crack density attains 0.99/mm but moderate crack density in the upper region.

Experiment 04077.1

This experiment had an initial oxide layer thickness of 300 μm but shows only a low crack density (Fig. 32) between 35 and 63 mm. The crack lines are accompanied by black stains like beads on a chain. The black stains have the same appearance as seen already in experiment 11047.

Experiment 08077.1

Between 27 and 125 mm this experiment (Fig. 33) shows different crack patterns. From bottom to the center the cracks are more or less circumferential. In the upper half two long axial cracks dominate the crack pattern. Crack density varies from 0.22 /mm to 0.42 /mm.

Experiment 08077.2

This experiment is shown in two figures (34 and 35) covering the length between 25 and 117 mm. The crack patterns are dominated by two long rather straight axial cracks with many circumferential cracks crossing the axial cracks at 90° angles.

8. Crack density comparison

The crack densities of several pins from a series of recent experiments are listed in Table 1 and plotted as a function of the oxide layer thickness (Figs. 36 and 37). The penetrating cracks open new surfaces in the α -Zr(O) and β -Zr layers. For a layer of 0.3 mm thickness and a crack density of 1/mm the newly generated metallic surface is of the order of 30% of the circumference area.

The oxide layer thickness was measured optically on polished cuts. The crack density is the ratio of the line length generated by hand tracing and the surface area of one circumferential image assembly.

The automatically generated crack lengths mentioned in the text are bigger than the hand traced cracks. Since automatic tracing generates double lines in broad cracks and artefact lines in areas with low albedo, the hand traced crack densities are considered to be closer to reality. The variation of the crack density along the axis is considerable for the pins which were traced over the hot length. The crack density of the other specimen was measured only from a narrow 15-30 mm wide circumference image. It seems that the dependence of the crack density from the oxide layer thickness resembles a step function with a critical oxide thickness between 190-210 μm by steam cooldown at 1200°C and between 220-230 μm at 1400°C (preliminary results can be seen in Table 1).

9. Conclusions

The assembling of axial or circumferential views of the test pins is now possible with an electronic camera system and a motorized positioning system. The axial mosaic images show the influence of the temperature field and initial oxide layer thickness on the cracking behaviour of the tube. The circumferential mosaics show an unwrapped 360 degree circumference of the pin. Most of the spatial and contrast distortions caused by curvature and parallax are corrected and allow to extract quantitative information about albedo and crack density of the surface.

Polarized light and a solvent or liquid penetrant are necessary to visualize hidden cracks in the tube surface. The polarized light suppresses also reflections from certain angles of the curved tube surface. The solvent or penetrant indicates where cracks are penetrating from the inner to the outer surface of the tube.

The circumferentially integrated reflectivity of the tubes showed similar patterns along the axial coordinate for (*only*) two experiments: white rings at about 20 mm from the ends and low reflectance in the hot region.

Algorithms have been developed which generate a net of lines representing different classes of cracks. The penetrating cracks visible after solvent injection are traced also by hand (mouse input). The automatic tracing with acetone.mac showed 200 to 300% higher crack length than hand tracing. The macros may be improved with further features (suppression of short lines, double lines, horizontal or vertical lines), but for the moment it is believed that hand tracing is more reliable despite being more subjective.

Until so far the interdependence between visible cracks, oxide reflectance and oxide layer thickness has been verified for some points only. Some pieces of broken tubing allowed visualization of crack lines on both sides of the tube. The new eddy current device allows measurement of the oxide thickness nondestructively and to detect cracks in the α -Zr(O) via an increase of the thickness signal.

10. Acknowledgment

We would like to thank Dr. P. Hofmann (FZK) and Dr. T. Haste (AEA Technology, UK) for this thorough review of the paper.

Table 1. Experiments with cooldown by steam.

Preoxidation in steam by 1400°C at flow rate of 0.08 g/s.

Probe	Preoxidation			Cooldown		Crack analysis			
	Time	ZrO ₂ thickness optic measurement*	ZrO ₂ thickness. eddy current**	V _{steam}	from	Coord. from bottom	Step	Crack density, mm/mm ²	
	min	µm	µm	g/s	°C	mm	mm	Distribution	Mean
200272	30	230(30mm) 260-285(57mm) 300(115mm)	259	0.08	1400	70-112		0.85;0.99;0.67; 0.48;0.57;0.31	0.65
210271	35	260(28mm) 300(55mm) 300-430(118mm)	315	0.08	1200	95-110	-	0.55	0.55
270271	30	230(27mm) 310-420(77mm) 300-430(125mm)	306	0.08	1600	68-82	-	0.46	0.46
030372	7	150(33mm) 140(70mm) 160(120mm)	146	0.08	1200	20-130	-	2 axial cracks	0.06
030371	15	180-200(80mm) 230(115mm)	198	0.08	1200	87-119	14	0.46;0.45	0.46
080471	15	190-200(32mm) 195-220(55mm) 200-225(100mm)	202	1.5	1200	55-125	-	2 axial cracks	0.06
090471	15	195(43mm) 200(85mm)	197	0.08	1200	30-125	-	2 axial cracks	0.06
090472	20	225-240(30mm) 220(50mm) 220-240(100mm)	207	0.08	1200	20-118	14	0.52;0.66;0.42; 0.42;0.42;0.30	0.46
100471	20	220(66mm) 240-250(110mm)	242	1.5	1200	27-101	14	0.33; 0.40; 0.45; 0.57; 0.77	0.50
020771	10	135(56mm) 150(109mm)	144	1.5	1400	90-130		2 axial cracks~40mm, 1ax.crack~10mm	0.06
030771	15	180-200(97mm)	189	1.5	1400	20-130	-	2 axial cracks	0.06
030772	22	270(72mm)	235	1.5	1400	20-130	-	3 axial cracks	0.09
040771	30	270(101mm)	286	1.5	1400	35-63	14	0.35;0.35	0.35
080771	20+2	250(47mm)	248	1.5	1400	41-125	14	0.42;0.35;0.29; 0.34;0.22;0.34	0.33
080772	22	220(56mm)	221	0.08	1400	25-120	14	0.35;0.32;0.48; 0.35;0.30;0.36;0.42	0.37

*axial elevation in brackets

**mean value along tube from 50 points for each pin

Appendix A

A1

```
/* =====collfit.mac=====
Copyright (c) 1997 IBEX, IMF,FZK GmbH
Reads a series of adjacent subimages,
calculates the best matching lines at the edges
and assembles a composite image covering the circumference
=====*/

Delete(FileName,Name);
CHAR FileName[22,40]=" ", Name[40] = " ";
BYTE pixels[50,1000],pixel[50,1000];
INTEGER idel[15]=0.;
REAL cor[50];

newImage("SoftwareFixed","Kollage",1024:2816,NULL); /* generate empty image */

LoadFromOPTfile("c:/optimas6/config/ibex.cfg","pixel_cal");
Calibrate(pixel_cal); /* get calibration factors */

Name="d:/dampf ab_1400°C/080771/61.tif"; /* define starting name for image series */
top = 2560.; /*define subimage width and stepping difference */
delta=256.;
bottom=top - delta;
SelectROI(0:top:1023:bottom);

/* loop for reading the subimages into buffers and
and placing at equal distances */
fn="6162636465666768697071";
for(i=1;i<11;i+=1) { j=2*(i-1);
  Name[26]=fn[j];
  Name[27]=fn[j+1];
  FileName[i,]=Name;
  FileToList(Name);
  SelectROI(0:top:1023:bottom);
  ArithmeticOp("Copy",Name,);
  top=top-delta;
  bottom=bottom - delta; }

/*Loop for correlation analysis at the subimage interfaces */
top =257.;
bottom=207.;
for (ik=9; ik>0; ik+=-1) {
  SelectROI(24:top:1023:bottom);
  pixel=GetPixelRect(,pixels);
  REAL norm[50,1000] = ((REAL) pixels);
  normav= Reduce(norm,,1)/1000.;
  line0 = norm[0,] - normav[0] ;
```

```

abs0 = MatrixMultiply(line0,line0);

/* check lines no. 4 to 39 in next image */
cmax =0.;
for (i=1; i<49; i+=1) {
linei=norm[i,] - normav[i];
cori = MatrixMultiply(line0,linei);
absi = MatrixMultiply(linei,linei);
cor[i] = cori / Sqrt(abs0*absi);
neumax = Max(cmax, cor[i]); /* find best line correlation */
if (neumax>cmax) imax=i;
cmax=neumax;      }

/* store line number with best correlation */
idel[ik]=imax;
top=top+256.;
bottom=bottom +delta;  }
show (idel); /* show overlap values */

/*shift subimages to new positions where overlap is best */
newtop= (11*256) -Sum(idel);
top=255.;
bottom=0.;
for(i=10; i>0; i+=-1) {
  SelectROI(0:top:1023:bottom);
  Name=FileName[i,];
  ArithmeticOp("Copy",Name,);
  top=top+256.-idel[i-1];
  bottom=top-255.;    }

/* generate new region of interest covering 360 degree of circumference */
neutop=(10*256) -Sum(idel);
SelectROI(12:neutop:1011:0);

```

A2

```

/* ===== hellgrat.MAC =====
Copyright (c) 1996 IBEX, IMF, FZK GmbH
Author:   L. Steinbock
date:    21. 4. 1997
comments: generates line sceleton along bright ridges
=====*/

INTEGER xgradkern[5,5] =0..25;
INTEGER ygradkern[5,5] =0..25;
fhx= OpenFile("c:/filters/xgrat.asc");
fhy= OpenFile("c:/filters/ygrat.asc");

StatusBar = "Region select "; /* buffer the region of interest as "Rohbild" */
ActiveImage.ROIToList (, "Rohbild");

StatusBar = " ROI glaetten mit Gauss3x3 Filter "; /* average the image and buffering */
Filters(Gaussian3x3);

```

```

ActiveImage.ROIToList("gaus");

Histogram(); /* generate histogram and calculate the associated parameters */
cent=ArROIHistogramStats[5];

/* read ridge filters and convolve, first x then y ridge */
divisor=512;
offset=-cent*cent;
xtext = ReadFile(fhx,150); /* x-Grat-Filter lesen*/
nx=FromText(xtext,xgradkern,,25);
ActiveImage.Convolve(ROI,5,5,xgradkern,divisor,offset); /* Filter-Faltung */
ActiveImage.ROIToList("x");
ArithmeticOp("Multiply","x");
ActiveImage.ROIToList("x2"); /* Quadrat der X-Grate */

/* recall of averaged image and y ridge filter */
ArithmeticOp("Copy","gaus"); /* Rohbild holen */
ytext= ReadFile(fhy,150);
ny = FromText(ytext,ygradkern,,25); /*y-Grat-Filter lesen */
ActiveImage.Convolve(ROI,5,5,ygradKern,divisor,offset);
ActiveImage.ROIToList("y");
ArithmeticOp("Multiply","y"); /* Quadrat der y-Grate */
ActiveImage.ROIToList("y2");
ArithmeticOP("Add","x2"); /* x- und y-Gratquadrate addieren */
ActiveImage.ROIToList("grat");

/* thresholding, skeletonizing and object extraction */
Threshold(128:255); /* nur die hohen Grate als Binrbild erzeugen */
CreateLine(,TRUE); /*Skelettlinien der Grate erzeugen */
MultipleExtractAll(); /*Alle Merkmalsklassen extrahieren */

/* regenerate original image and close filter files */
ArithmeticOp("Copy","Rohbild"); /* Original Bildfenster regenerieren */
CloseFile(fhx); /* Filter-Dateien schließen */
CloseFile(fhy);

```

A3

```

/* ===== aceton.MAC =====
Copyright (c) 1996 IBEX, Inc.
author: 1. Steinbock
date: 14. 4. 1997
comments: generates line sceleton of cracks filled with solvent
===== */
INTEGER Grenzwert =0;

/* save the actual ROI on the image stack */
ActiveImage.ROIToList(, "Rohbild");
circle = 0:0:1:1:1:0:0:
          0:1:1:1:1:1:0:
          1:1:1:1:1:1:1:
          1:1:1:1:1:1:1:

```

```

1:1:1:1:1:1:1:
0:1:1:1:1:1:0:
0:0:1:1:1:0:0:
GrayErode(7,7,circle); /* gray erosion with circular pattern */
InvertFilter(); /* inversion of image */
Filters(Gaussian5x5); /* gaussian averaging */
Histogram(); /* calculate histogram */
mean = ArROIHistogramStats[0];
Threshold(); /* adjust threshold */
CreateLine(,TRUE); /* create lines */
ArithmeticOp("Copy","Rohbild"); /* regenerate original image */
DeleteImage("Rohbild"); /* clear buffer */

```

A4

```

/*=====craclang.mac=====
Copyright (c) 1997 Stuckert, IMF
calculate number of lines,
total length, line density
=====*/
LoadFromOPTfile("D:/Dampf ab_1400°C/juri.cfg","vergr10");
Calibrate(vergr10); /* get calibration factors */
CreateLine(,TRUE); /* clear existing, autcreate lines */
SetExport( mLnLength, 1, TRUE);
MultipleExtract(TRUE); /* classify */

linelang=0.;
for (i=0; i<LnTotalTally; i++) linelang = linelang + mLnLength[i];
statusbar = ToText(linelang);
Show("Number of lines are:",LnTotalTally,"\
Total length of cracks is:",linelang=linelang/1000,"mm");

rCenter = ConvertPixelsToCalib(FGDDimensions/2);
ImageArea=rCenter[0]*rCenter[1]*4;
Show("ImageArea=",ImageArea=ImageArea/1000000,"mm*mm"); /*area of frame*/

CrackDensity=linelang/ImageArea; /*crack density in mm/mm2*/
Show("Crack Density=",CrackDensity,"/mm");

fh = OpenFile ("D:/Dampf ab_1400°C/craccdens.dat", 0x1002);
a = " ": ToText (CrackDensity);
PositionFile (fh, 0L, 2);
WriteFile (fh, a);
CloseFile (fh);

```

List of figures:

- Fig. 1 Image analysis system for the QUENCH experiments
- Fig. 2 Experiment # 2805, axial scanning from top to bottom at 4 different azimuthal angles
- Fig. 3 Experiment # 03037.1 with solvent injection for crack visualization
- Fig. 4 Experiment # 2805 on top of the central thermocouple with different crack patterns
- Fig. 5 Piece of pin # 2805 with laminar bands outside and open cracks in the α -Zr(O)-layer
- Fig. 6 Experiment # 19066 with bleeding red liquid penetrant
- Fig. 7 SEM image of fractured Zircaloy tube with penetrating crack which is open inside and closed outside
- Fig. 8 Correction of reflectance variations, curvature and parallax by division with a reference image
- Fig. 9 Azimuthal scan with constant step angle
- Fig. 10 Intensity transformation and area generation for experiment # 2102
- Fig. 11 Filter effects demonstrated with a typical cracked part of experiment # 25086
- Fig. 12 Axial contiguous images of experiment # 10096
- Fig. 13 Average surface albedo of zircaloy tube quenched at 1400° C (Pin # 10096)
- Fig. 14 Open crack density of experiment # 10096 quenched at 1400° C
- Fig. 15 Closed crack density of a tube quenched at 1400 °C (experiment #10096)
- Fig. 16 Three consecutive circumference images of experiment # 28056
- Fig. 17 Crack lines calculated with acetn.mac from three images of experiment # 28056
- Fig. 18 Circumference image of experiment # 03037.2
- Fig. 19 Experiment # 03037.2 (1200° C, 200 μ m oxide layer thickness)
- Fig. 20 Experiment # 21027, (1200° C, 300 μ m)
- Fig. 21 Experiment # 19066 between 22 and 37 mm
- Fig. 22 Experiment # 19066 between 48 and 63 mm
- Fig. 23 Experiment # 19066 between 92 and 106 mm
- Fig. 24 Experiment # 19066 between 110 and 124 mm
- Fig. 25 Experiment # 19066 between 128 and 145 mm
- Fig. 26 Experiment # 05066 (1400° C, 300 μ m oxide layer thickness)
- Fig. 27 Experiment # 27027 (1600° C, 300 μ m oxide layer thickness)
- Fig. 28 Surface of experiment # 09047 (1200 ° C, 250 μ m oxide layer thickness)
- Fig. 29 Experiment # 10047, surface image and crack density
- Fig. 30 Experiment # 11047
- Fig. 31 Experiment # 20027.2, surface and crack pattern
- Fig. 32 Experiment # 04077.1, surface and crack pattern
- Fig. 33 Experiment # 08077.1, surface image and crack pattern
- Fig. 34 Experiment # 08077.2 (lower part), surface image and crack pattern
- Fig. 35 Experiment # 08077.2 (upper part), surface image and crack pattern
- Fig. 36. Crack formation in preoxidized Zircaloy during rapid cooldown at 1200°C.
- Fig. 37. Crack formation in preoxidized Zircaloy during rapid cooldown at 1400°C.

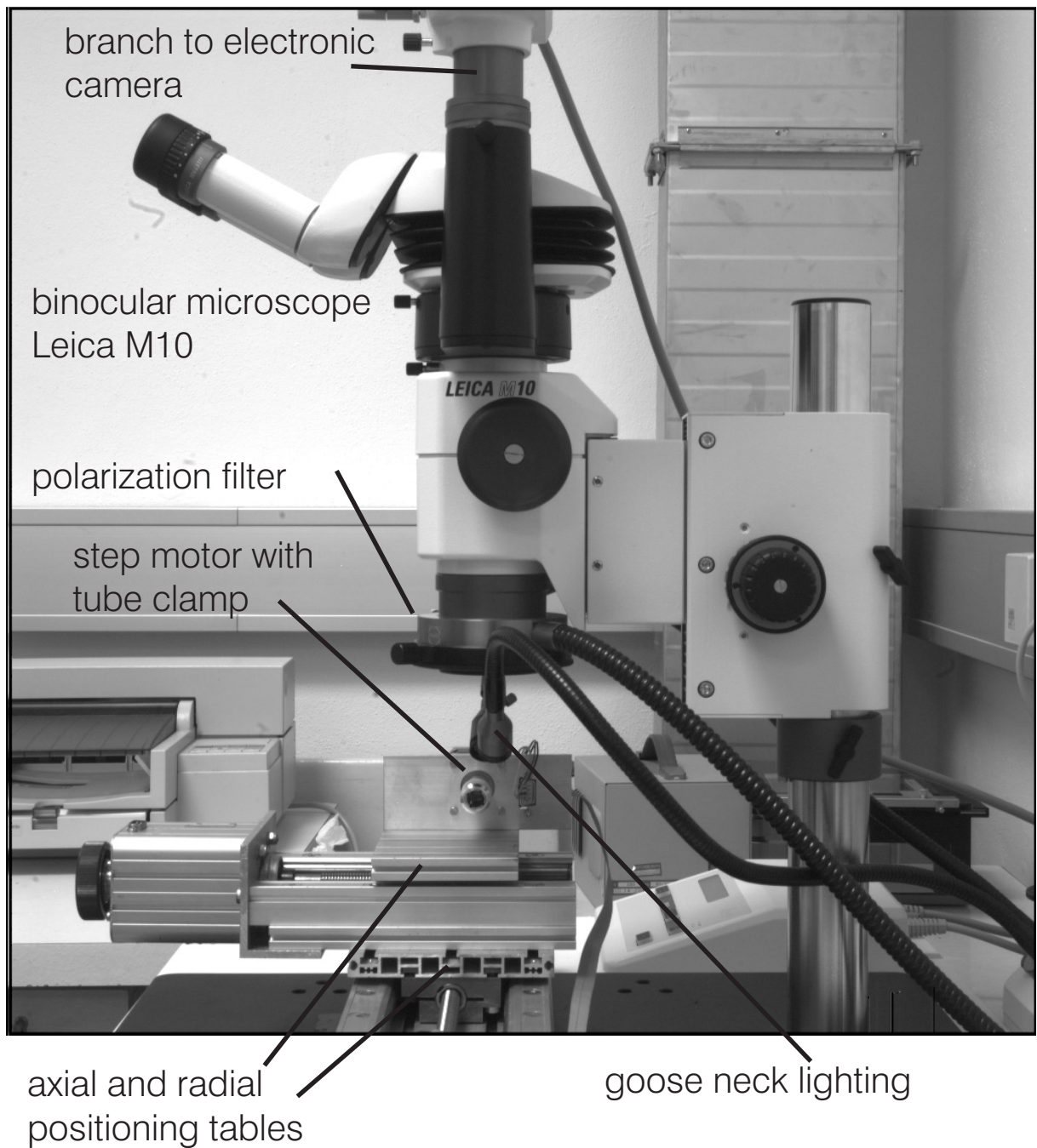
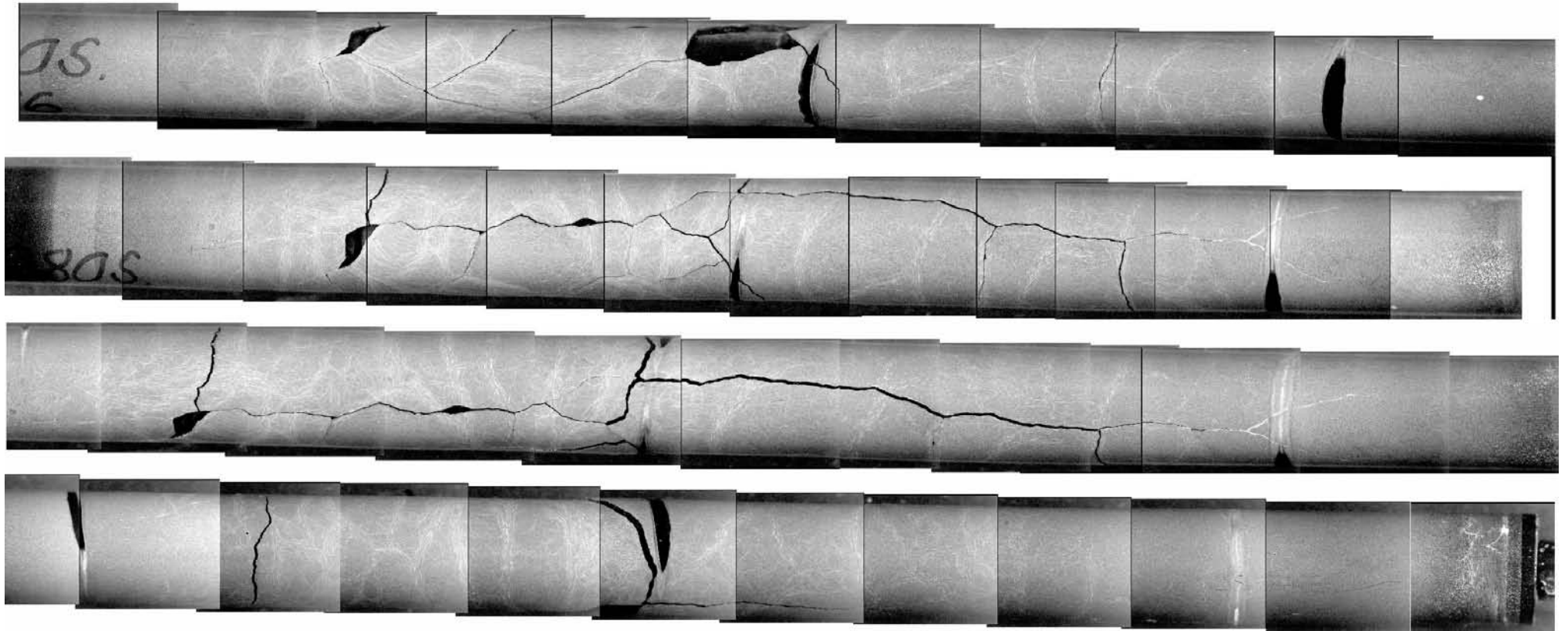


Fig. 1: image analysis system for the QUENCH experiments

<< top (150 mm)



bottom (0 mm) >>

Fig. 2 : experiment 2805, axial scanning from top to bottom at 4 different azimuthal angles assembled manually with Corel-Photopaint

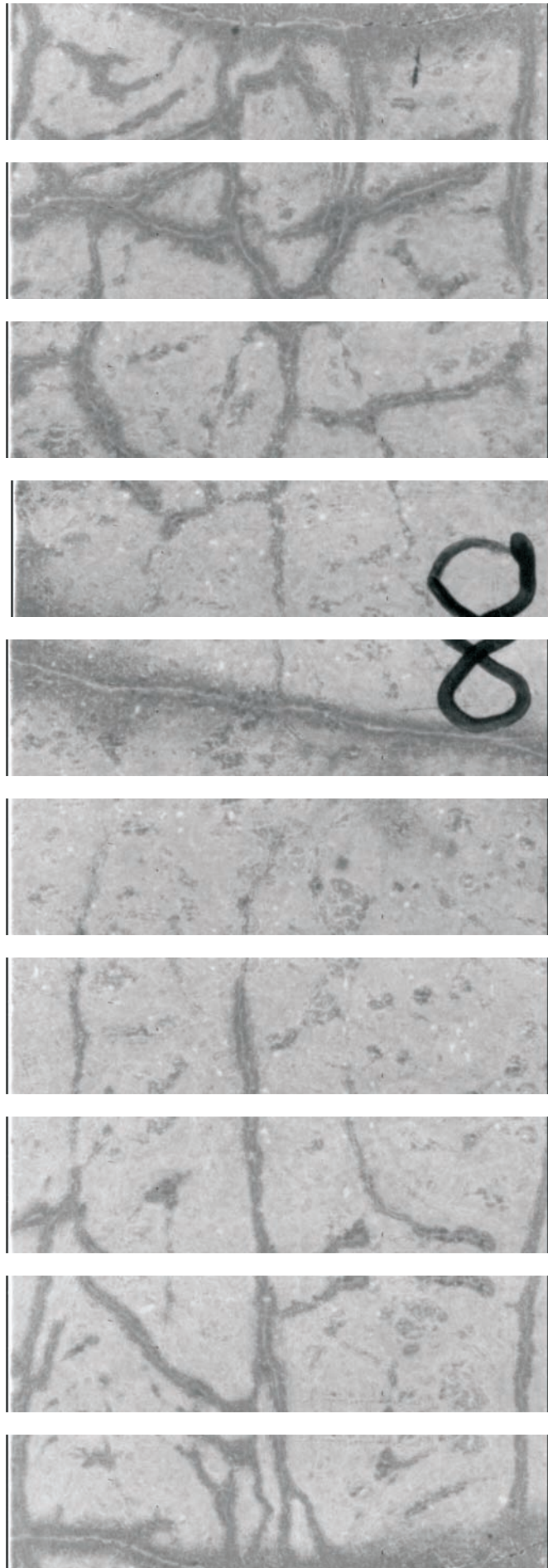


Fig.3: experiment 03037.1(1200°C quench temp.)with solvent injection for crack visualization, azimuthal scanning with 36° step angle

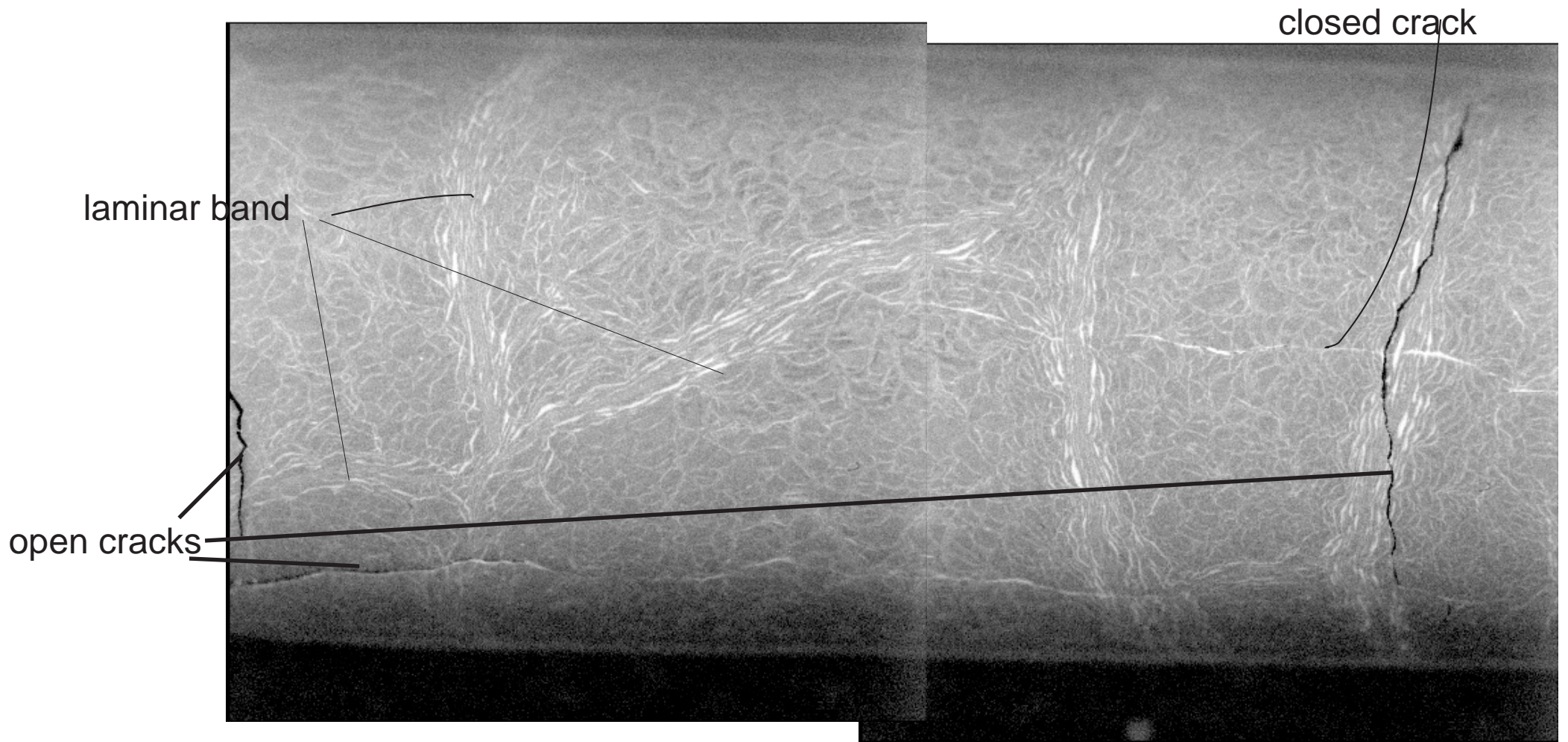


Fig. 4: experiment 2805 atop of the central thermocouple with different crack patterns, ring illumination with double polarization, no solvent, two overlapping subimages

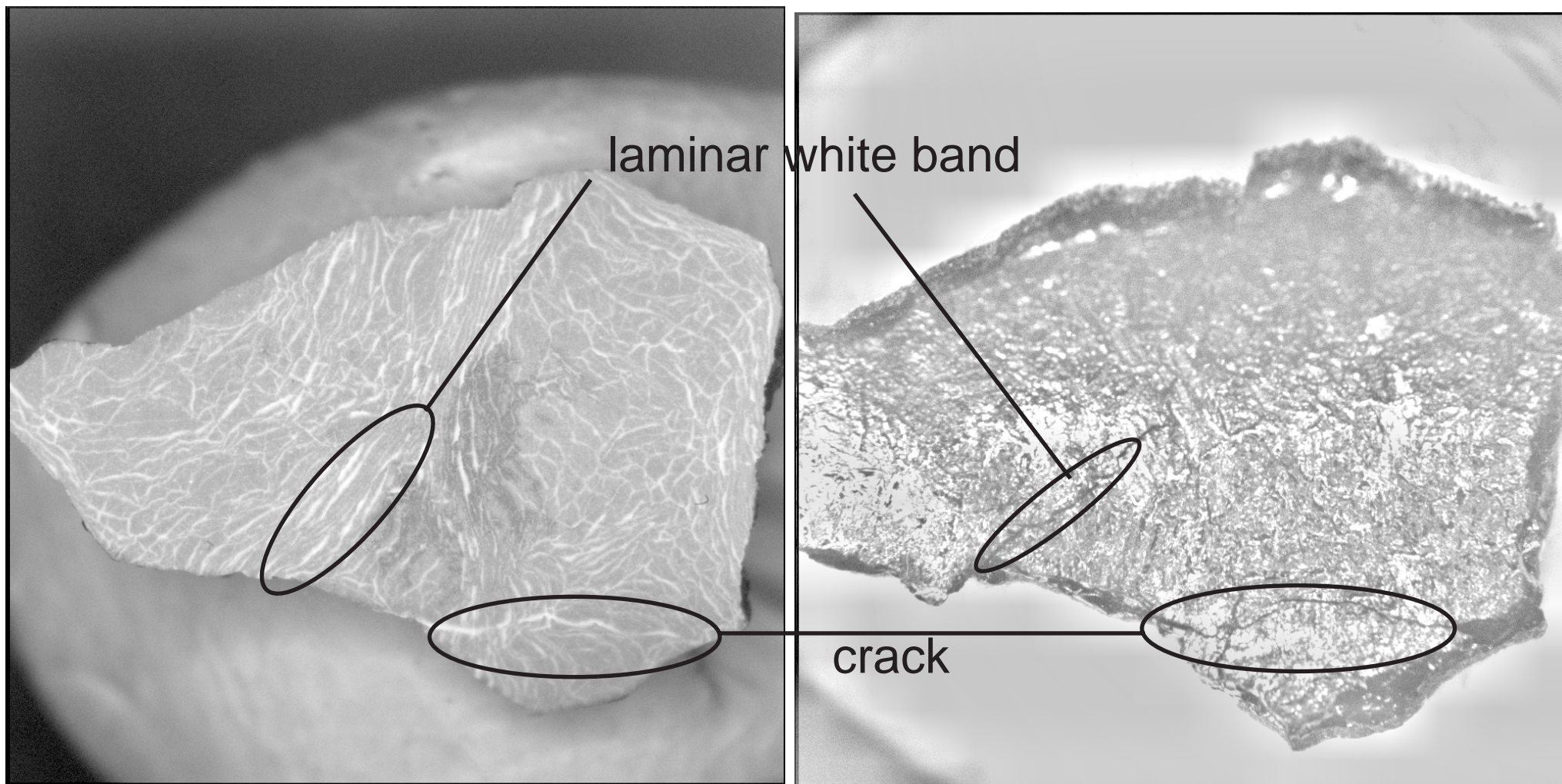


Fig. 5 : piece of pin 2805
with laminar bands outside (left) and

open cracks in the α -Zr(O)-layer (right)

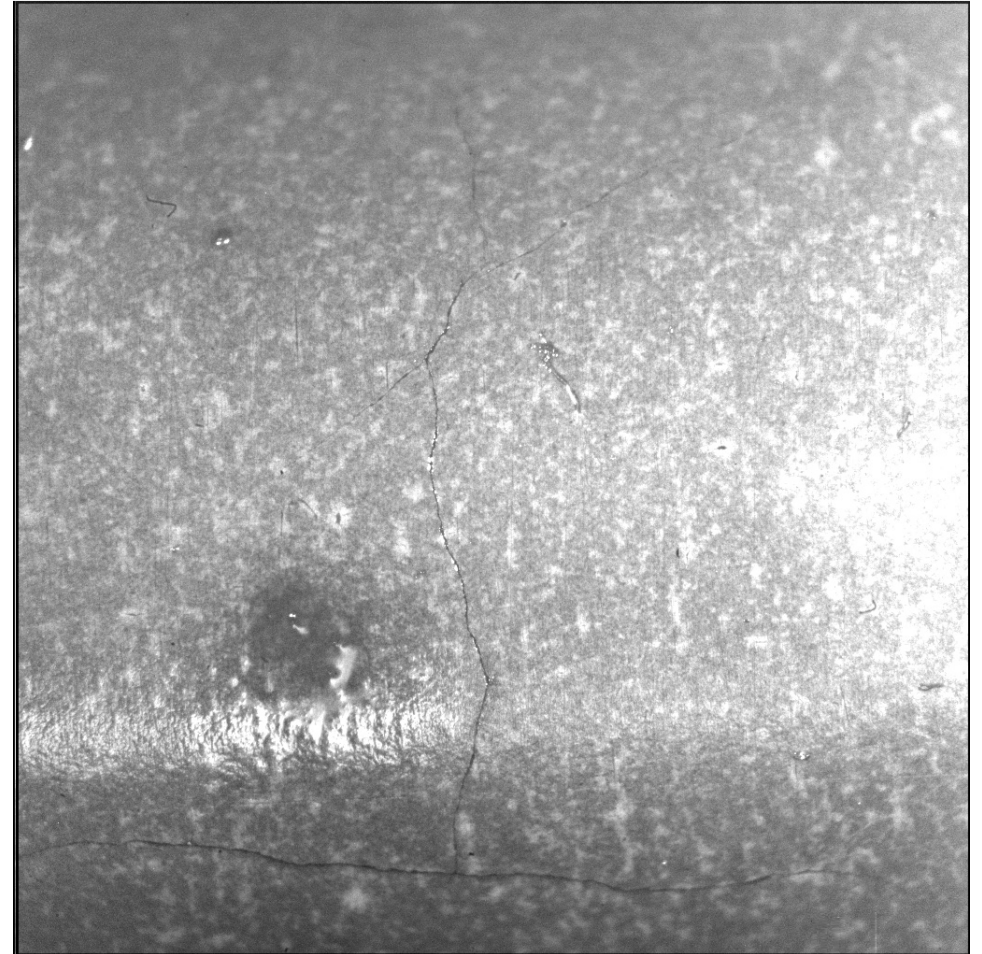
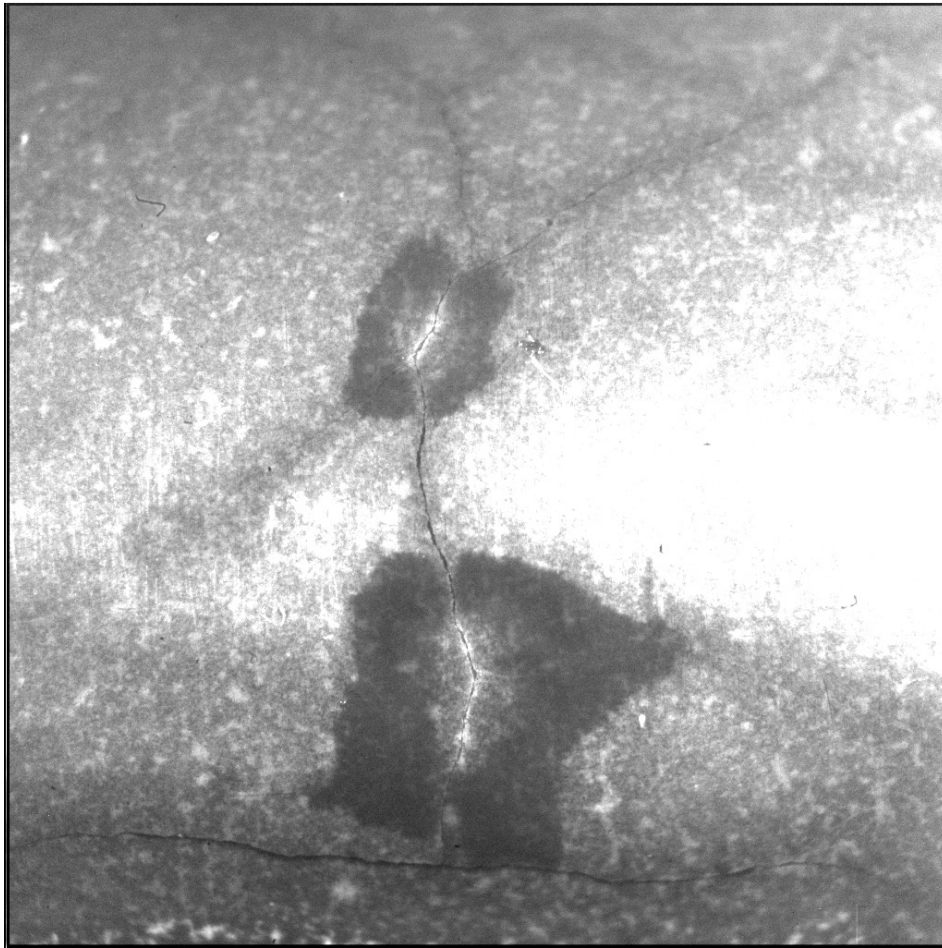


Fig. 6: Experiment Nr. 19066 (1600°C , $300\ \mu\text{m}$) with bleeding red liquid penetrant
left: 5 minutes after injection
right: after 16 hours of drying
illumination without polarization

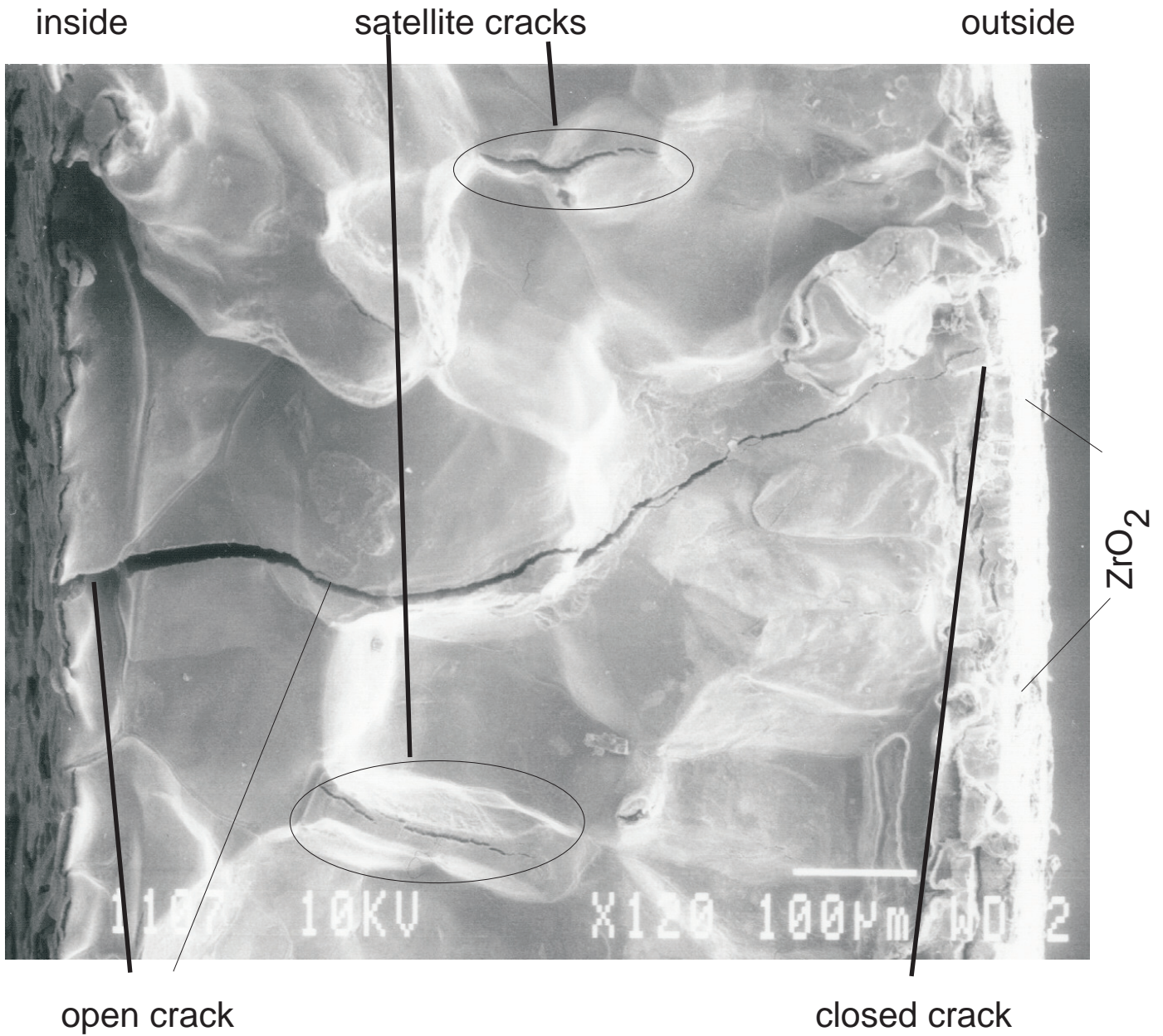
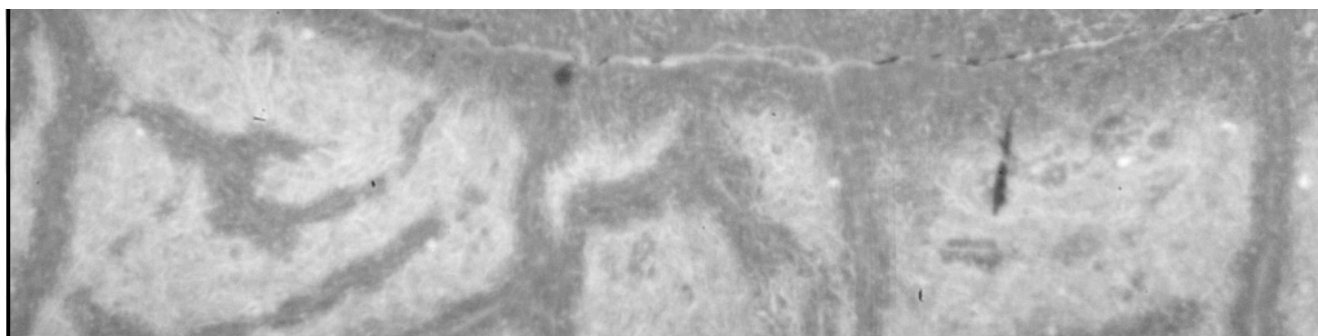
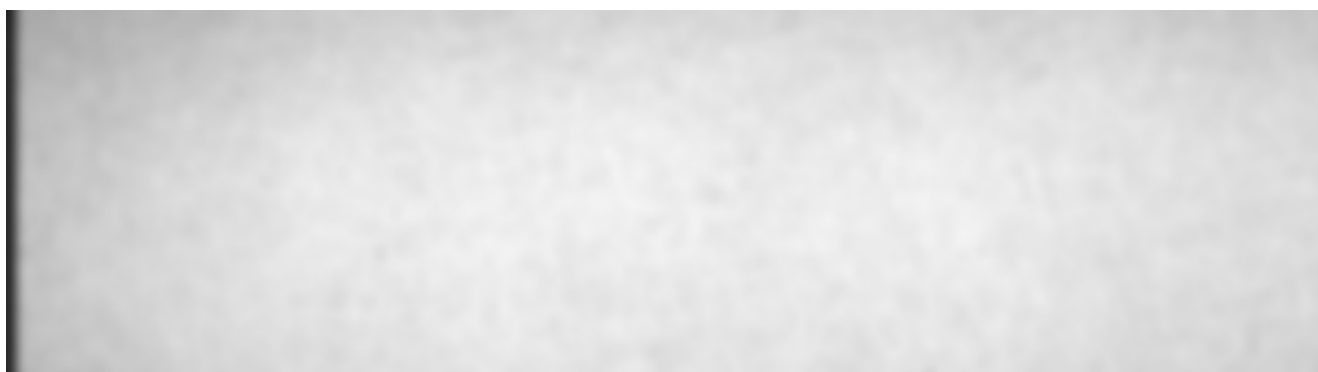


Fig. 7: REM image of fractured Zircaloy tube with penetrating crack which is open inside and closed outside

original image



reflectance of white paper on a 10.75 mm diameter tube



divided image

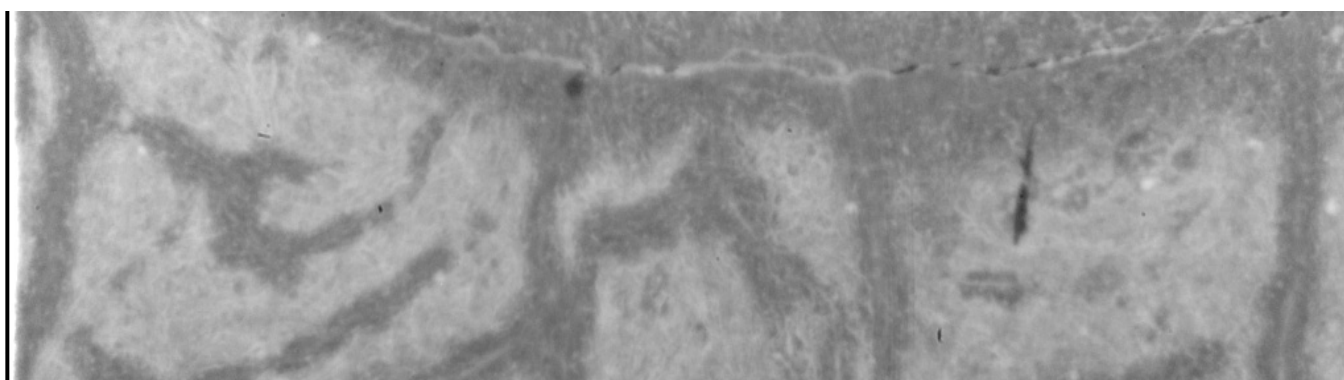


Fig. 8: Correction of reflectance variations due to illumination, curvature and parallax by division with a reference image

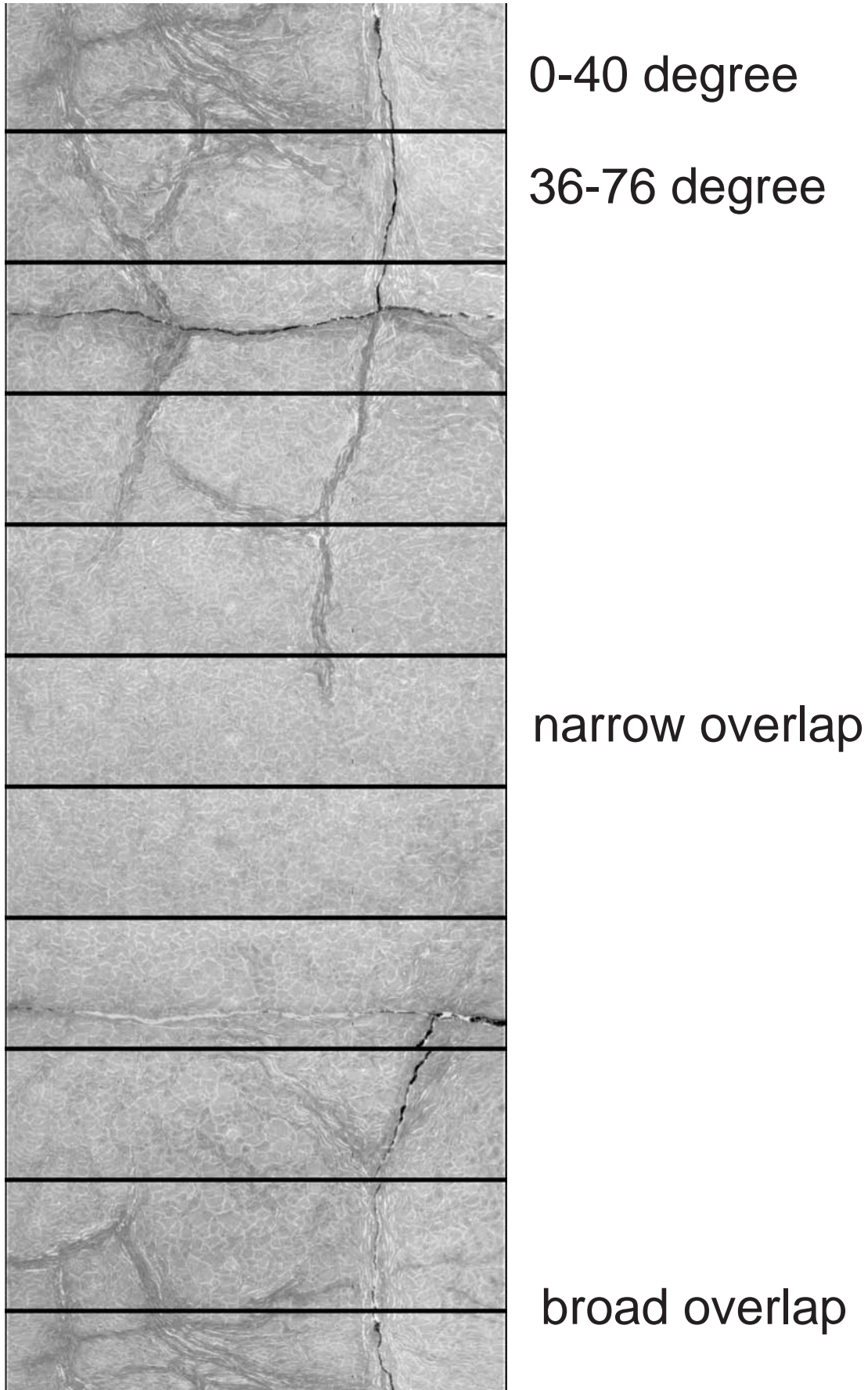


Fig. 9. azimuthal scan with constant step angle.
Varying overlap at edges of subimages due to eccentricity
and ellipticity of tube after the experiment

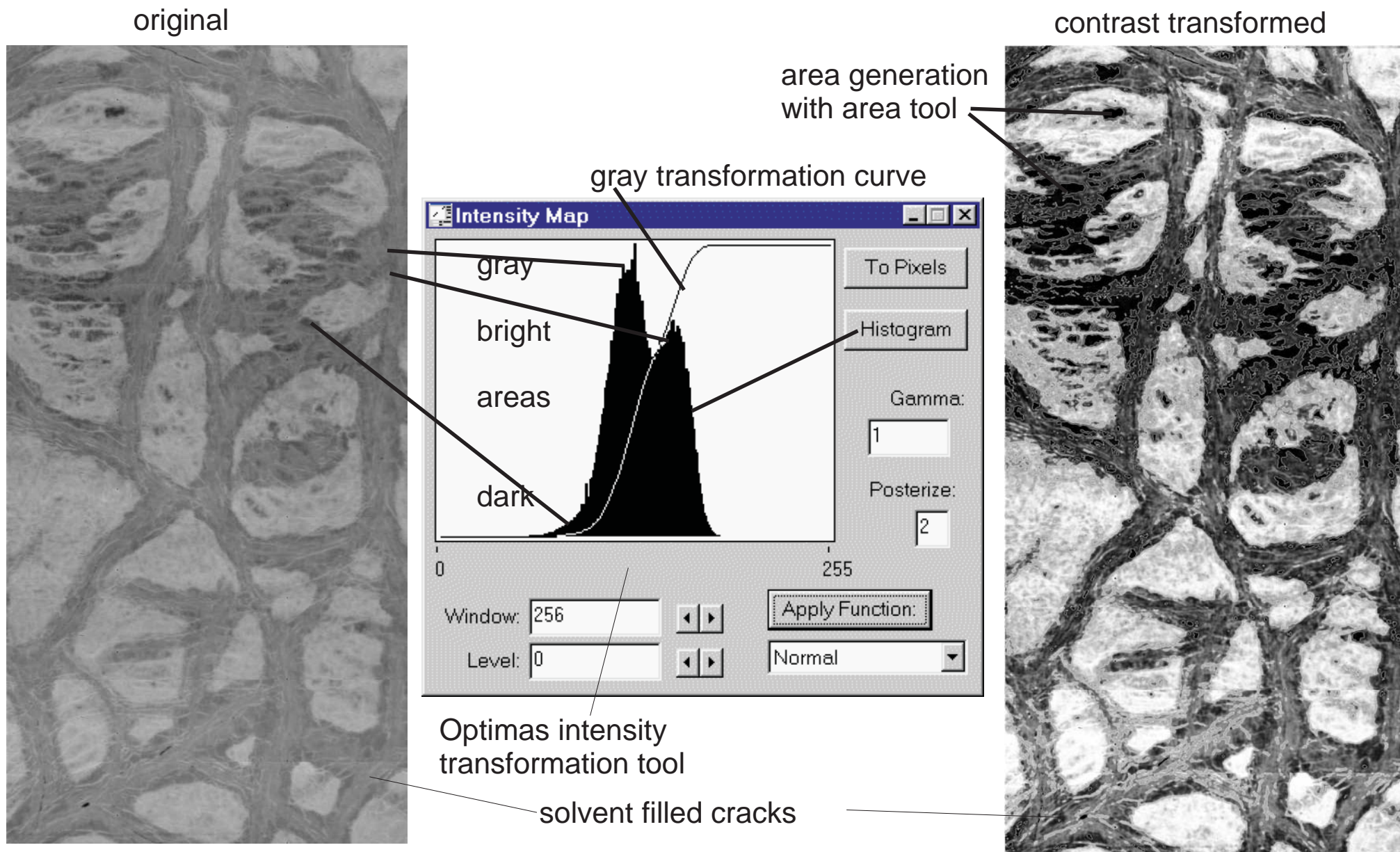
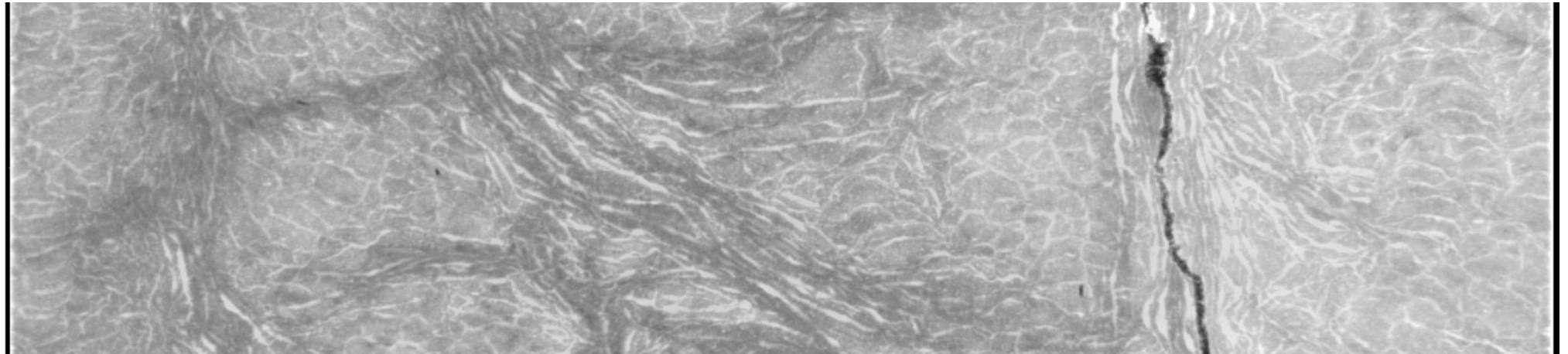


Fig.10 : Intensity transformation and area generation for cracks and stains of pin 2102



sharpening
filter (medium)

Sobel filter
(gradient)

hellgrat.mac

FFT

gaussian
averaging

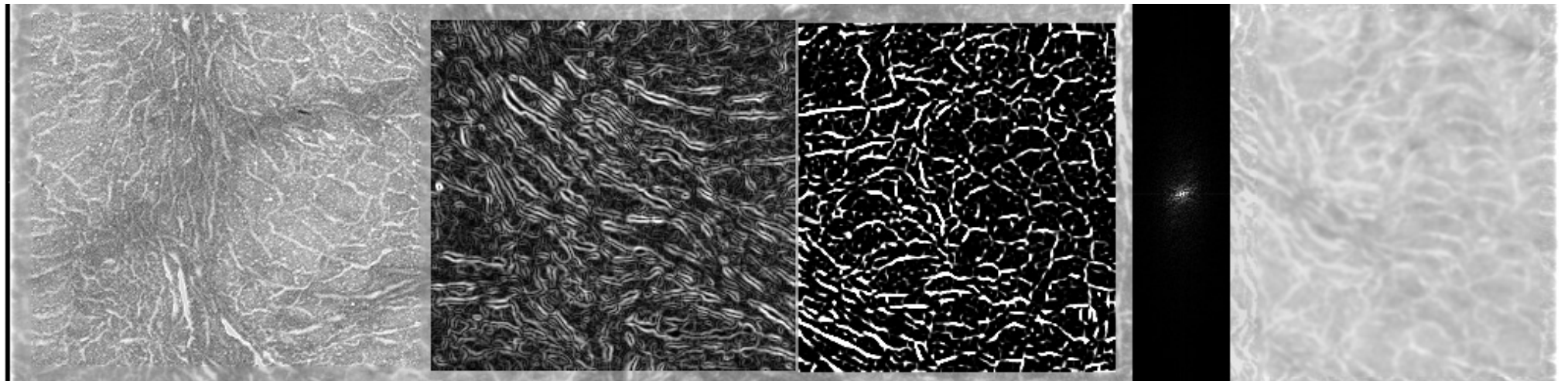


Fig. 11: Filter effects demonstrated with a typical cracked part of experiment 25086

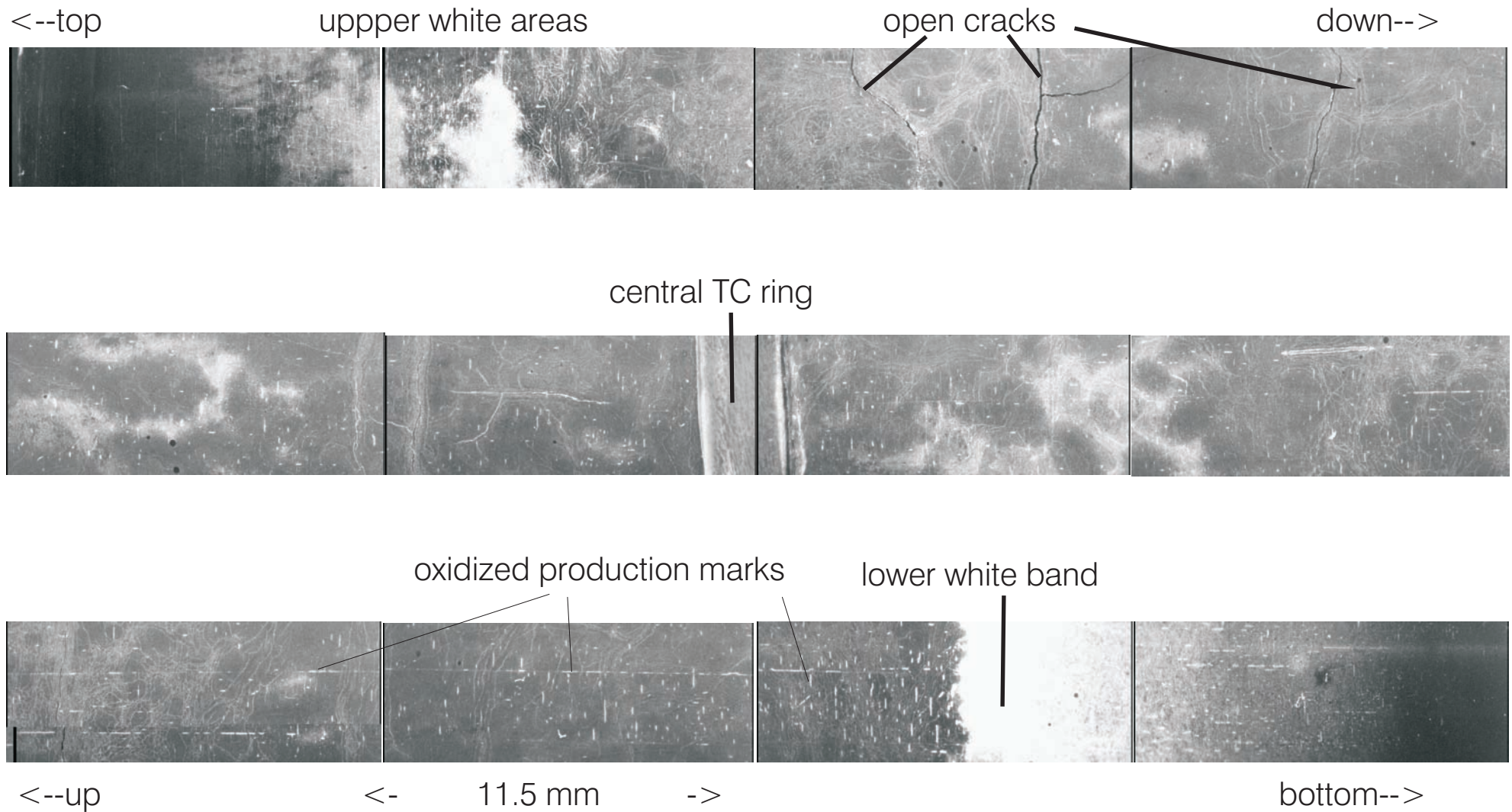


Fig. 12: Axial contiguous images of experiment Nummer 1009
 (water quenched from 1400°C with 300 μm initial oxide layer)

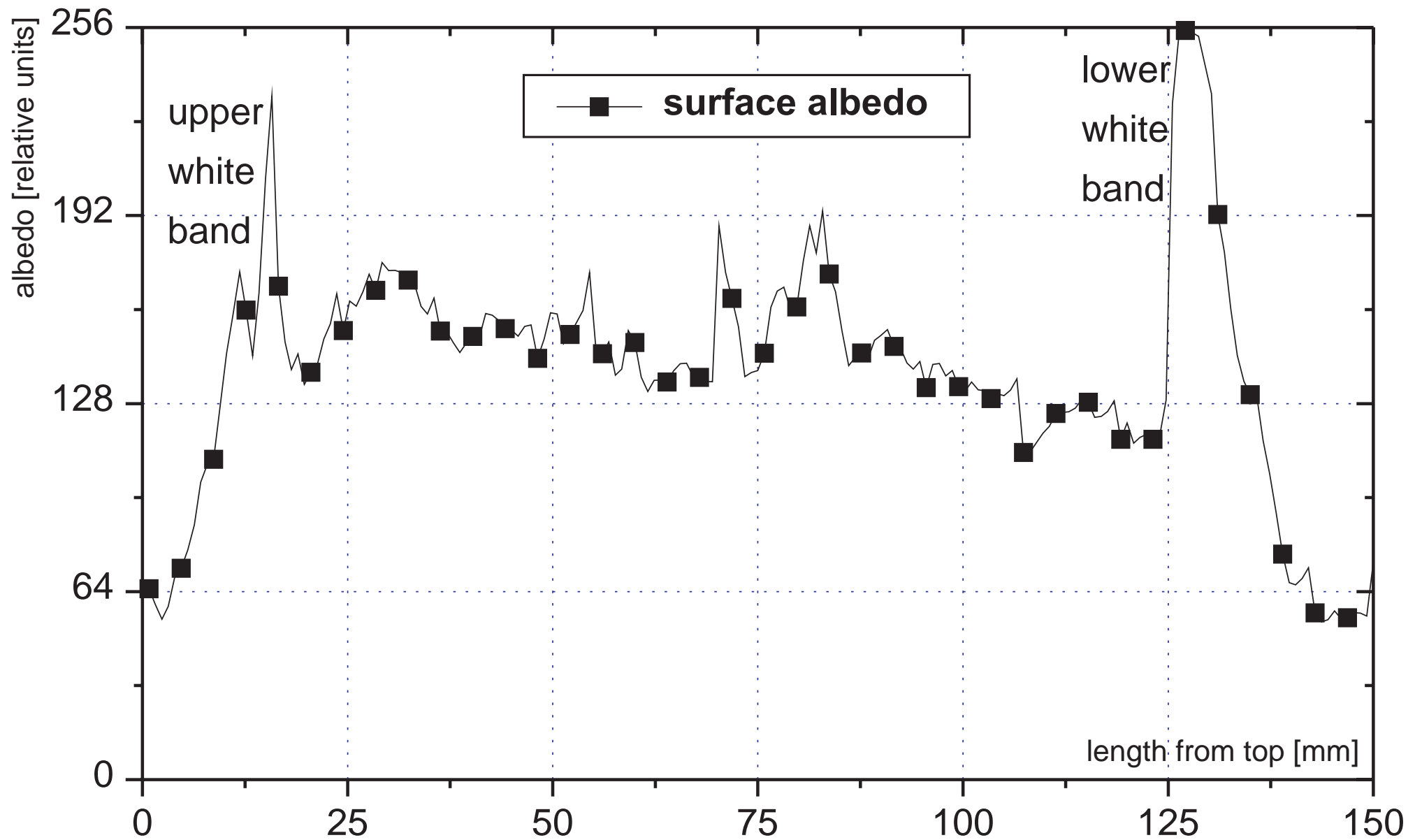


Fig. 13: average surface albedo of zircaloy tube quenched at 1400 C (Nr. 1009)

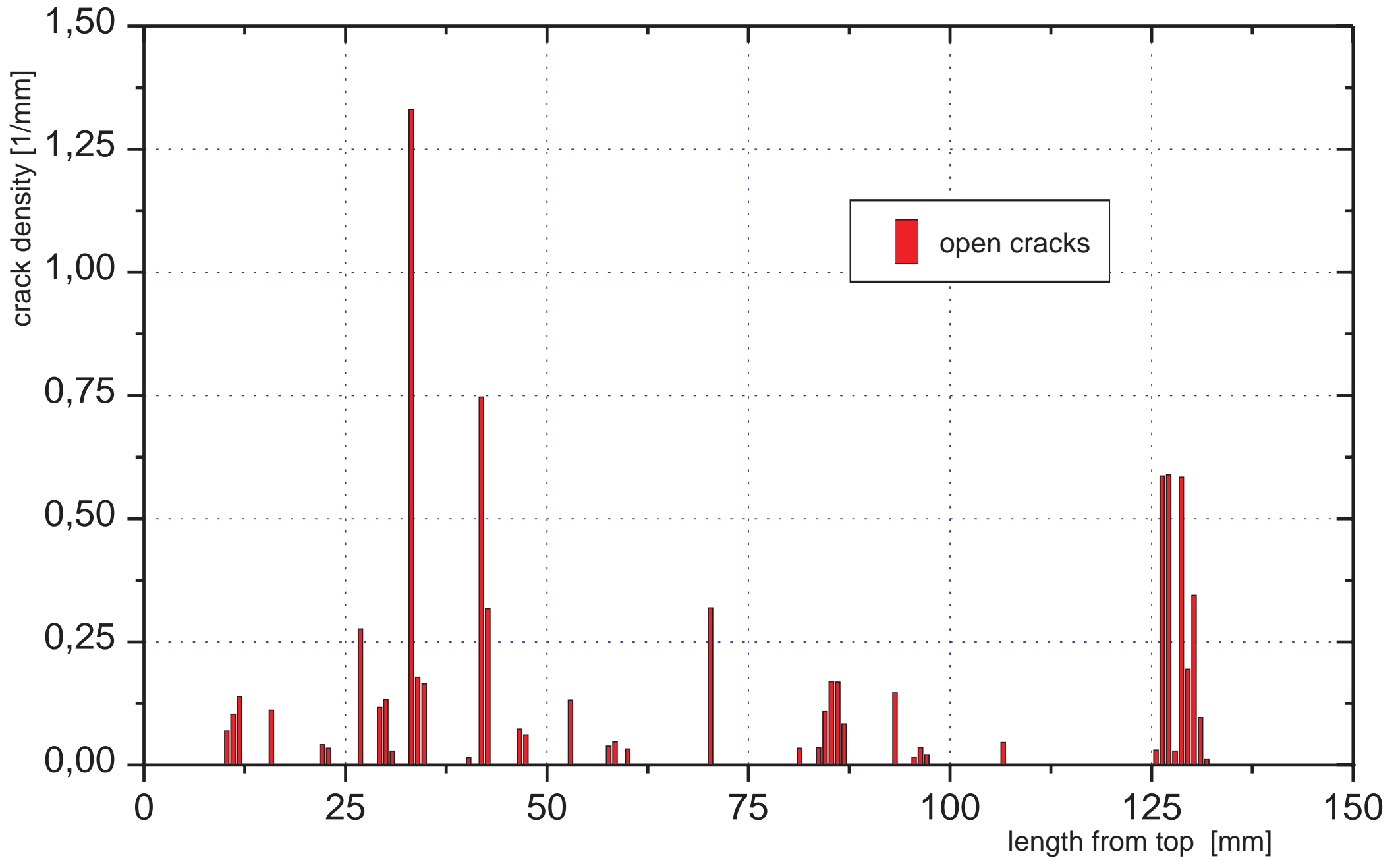


Fig. 14: open crack density of experiment Nummer 10096 quenched at 1400°C

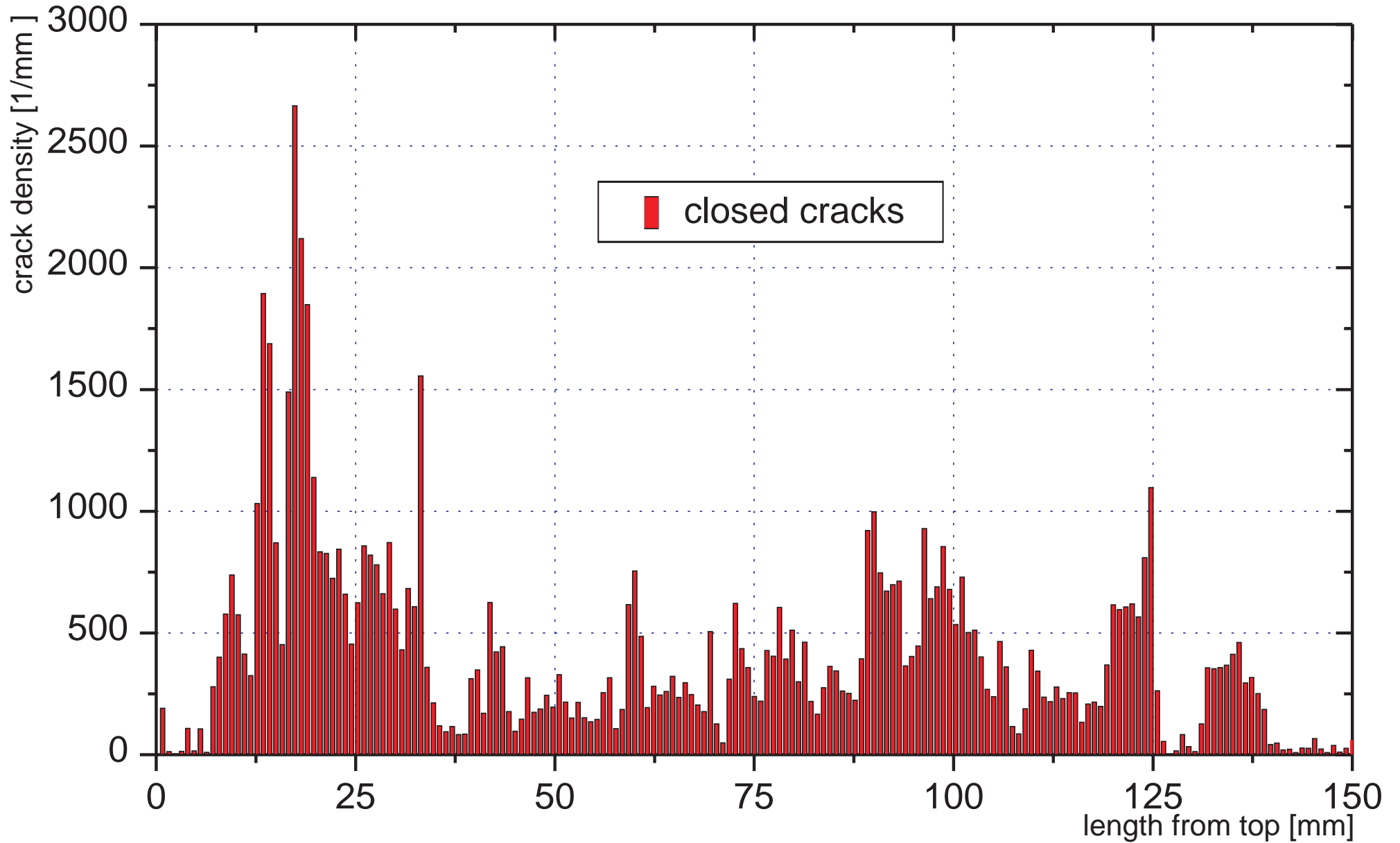


Fig. 15: closed crack density of a tube quenched at 1400° C (Experiment Nummer 1009)

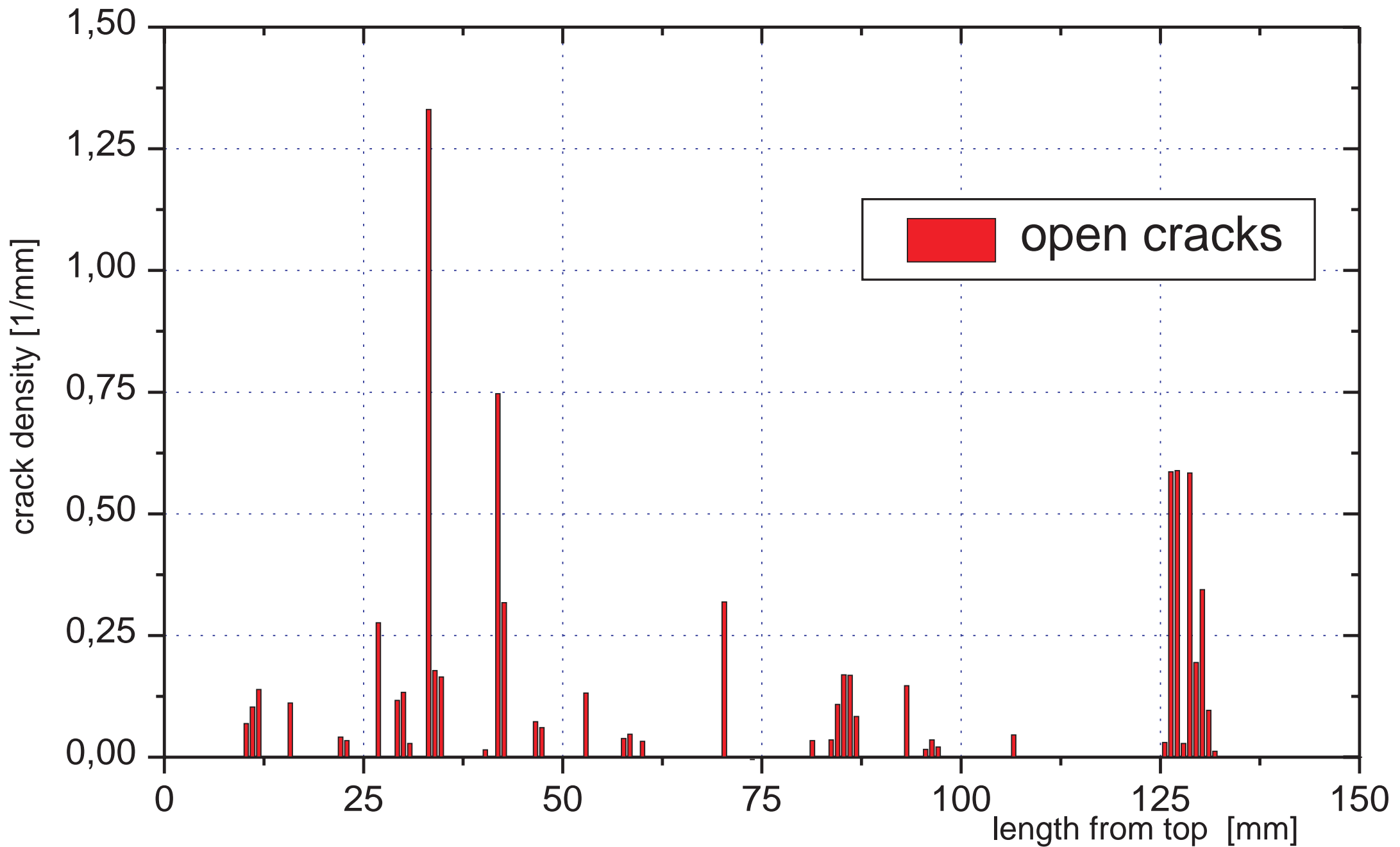


Fig. 14: open crack density of experiment Nummer 10096 quenched at 1400°C

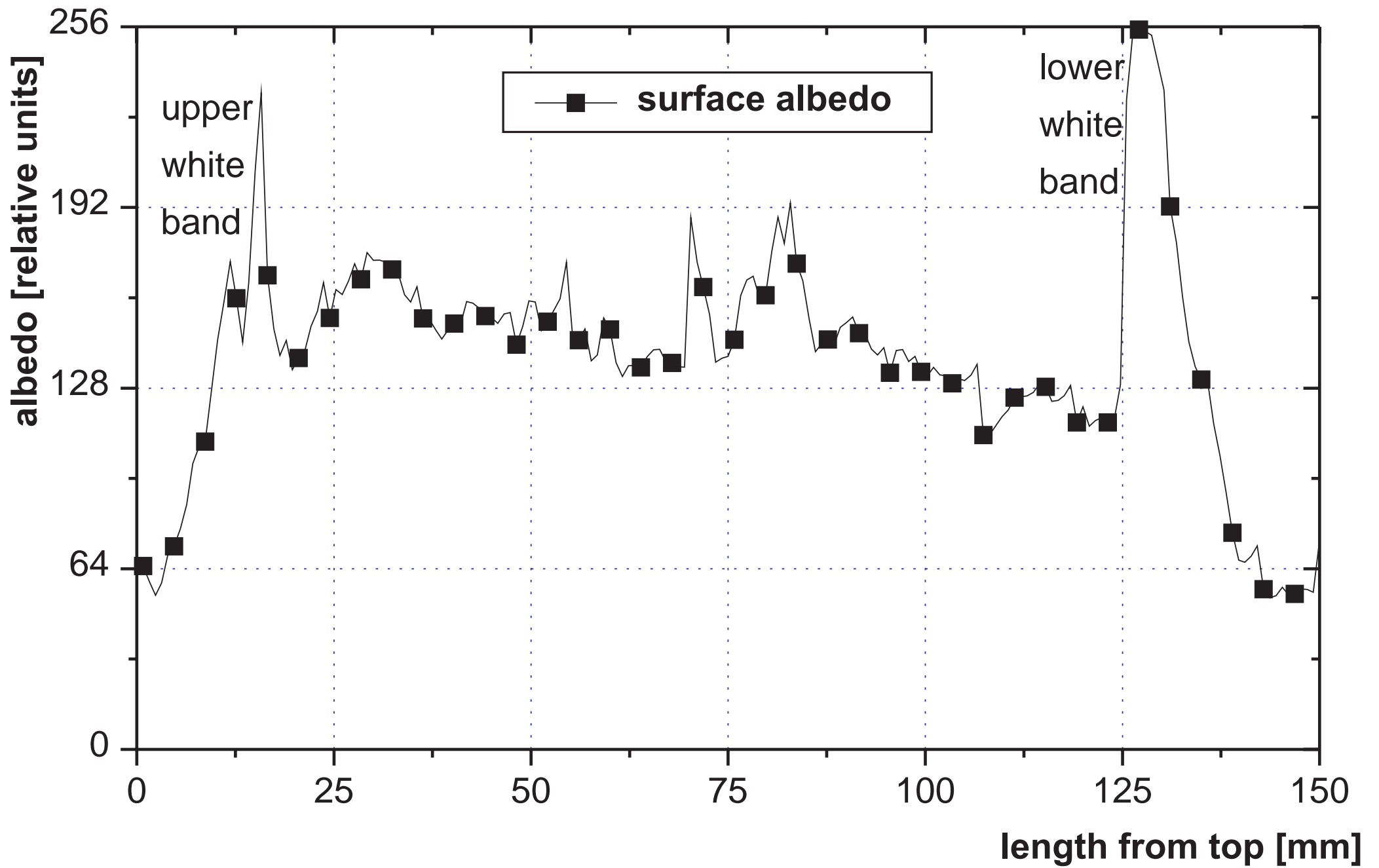


Fig. 15: average surface albedo of zircaloy tube quenched at 1400 C (Nr. 1009)

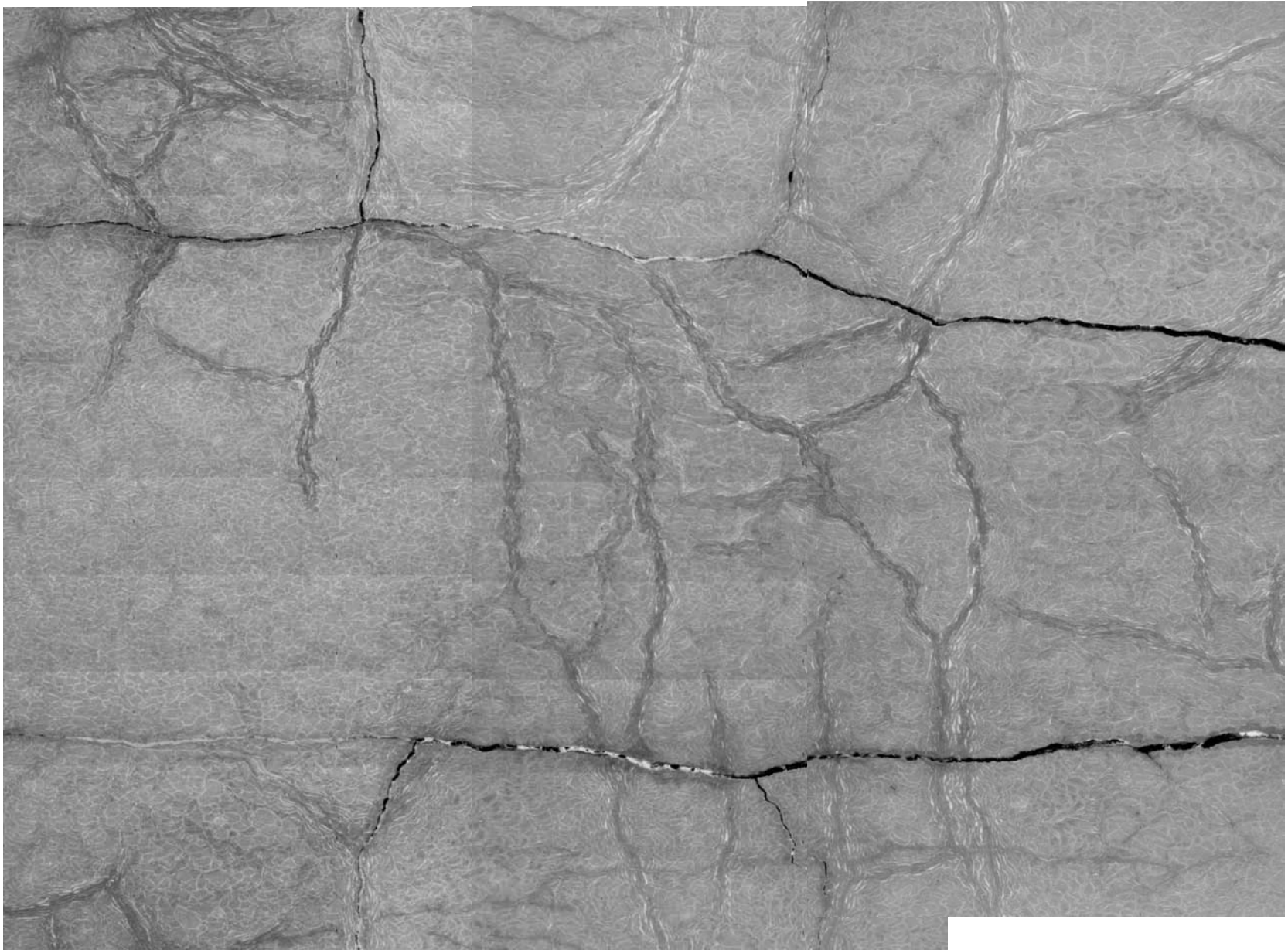


Fig.16: Three consecutive circumference (2pi) images of pin 28056 with liquid penetrant showing penetrating cracks

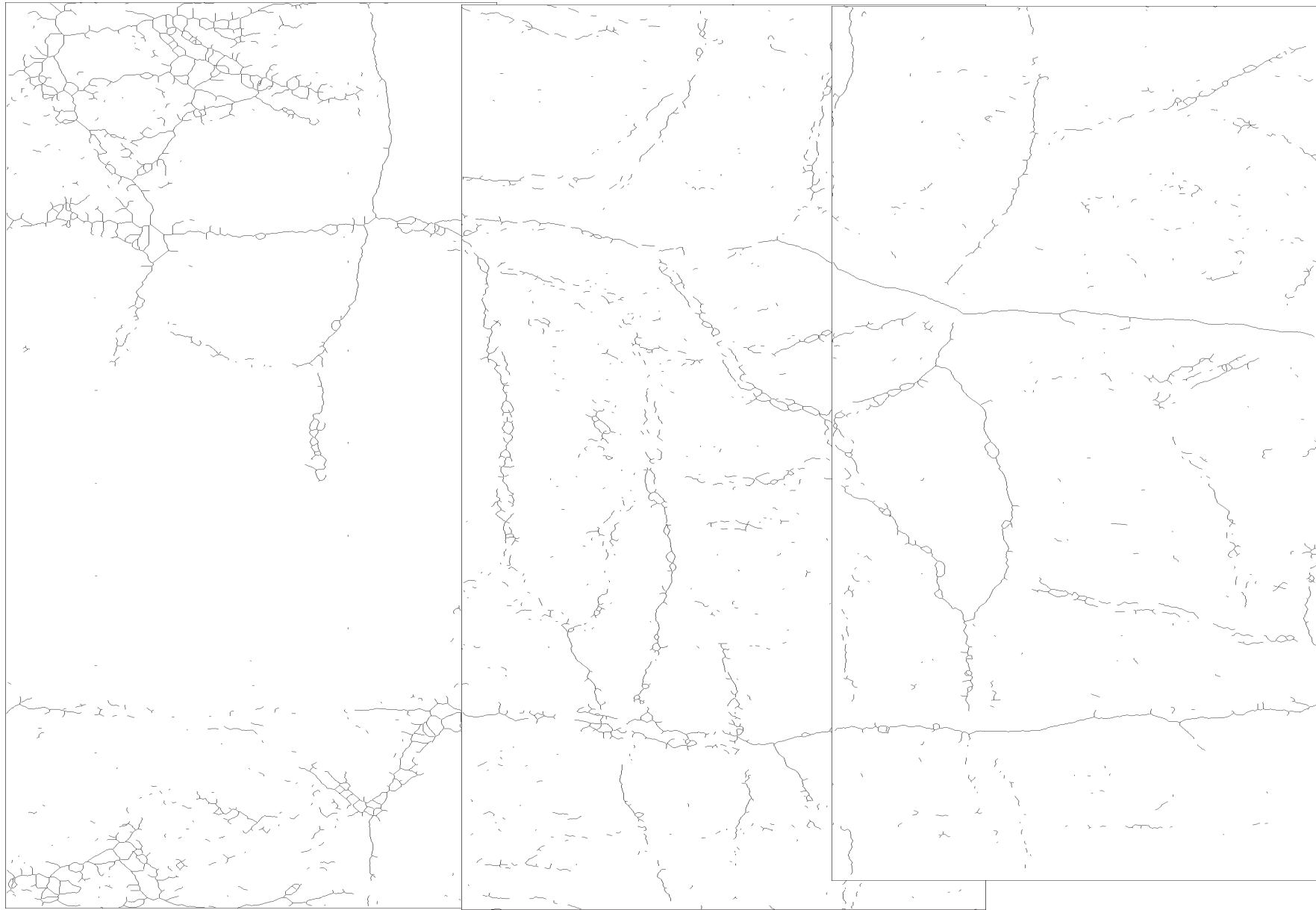


Fig.17: crack lines calculated with acetone.mac from three images of experiment 28056

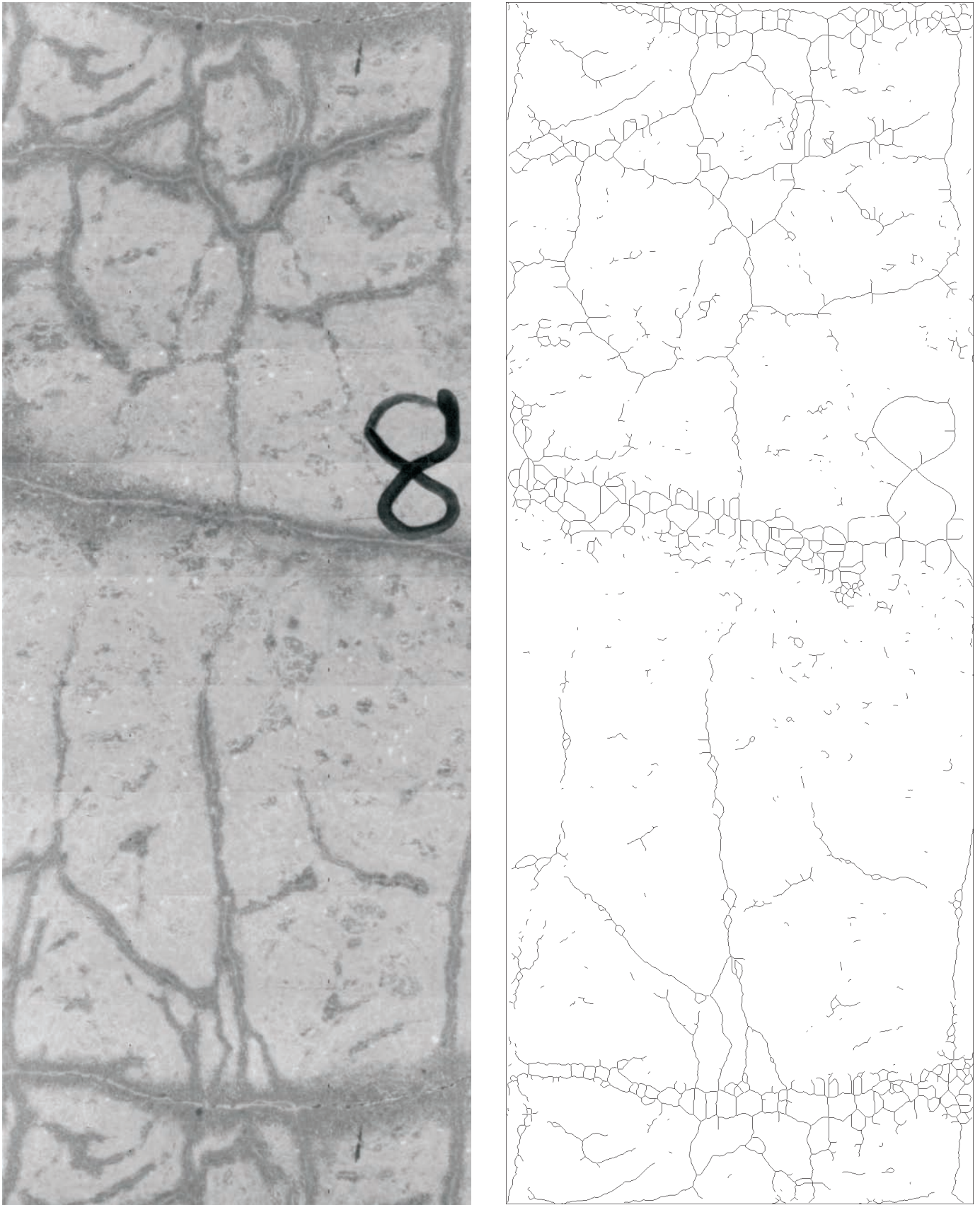


Fig. 18: experiment 03037.1 (1200° C, 200 μm oxide thickness)
circumference image ($\sim 400^\circ$) between 98 and 111 mm
left: albedo image after solvent injection,
right: crack lines generated with aceton.mac
815 cracks with 514 mm total length in 360° part of image

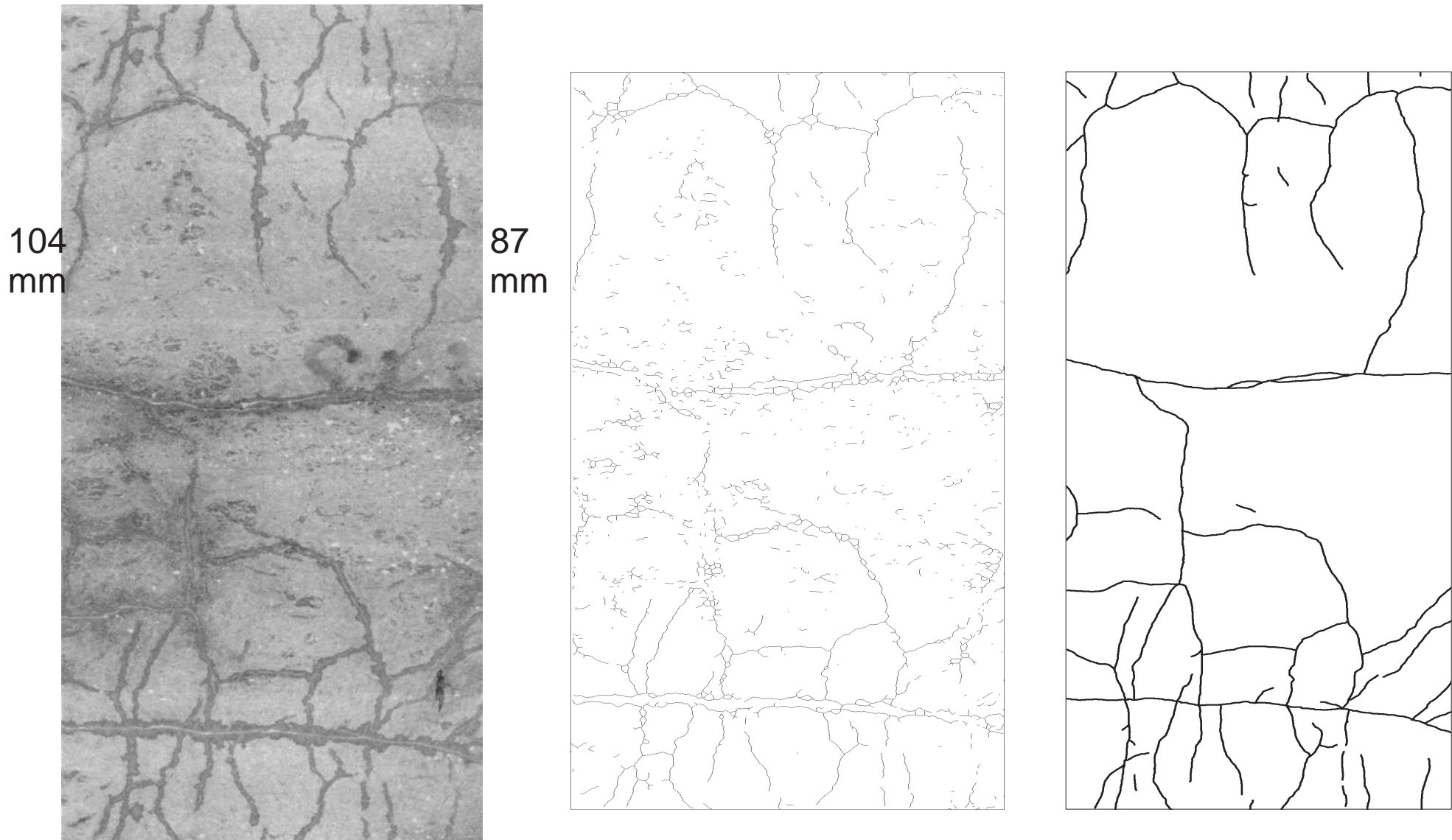


Fig. 19: Experiment 03037.1 (1200 °C, 200 μm oxide thickness)
left: circumference scan between 87 and 104 mm,
center: crack lines according to acetom.mac,
right: crack lines with hand tracing

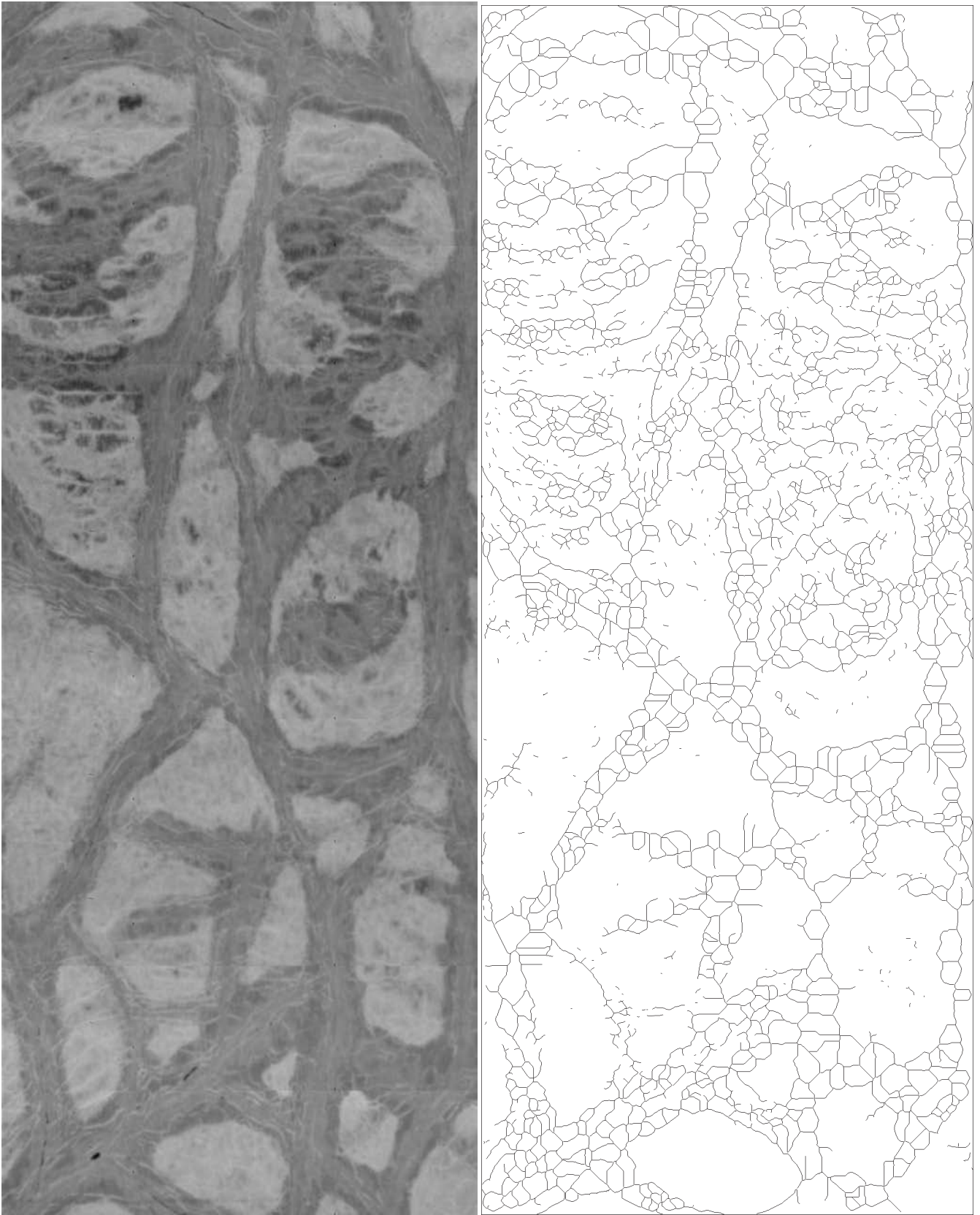


Fig. 20: Pin 21027.1 (1200 °C, 300 μm)

left: circumference image after solvent filling between 92 and 114 mm
right: crack lines generated with acetone.mac, total crack length 1118 mm

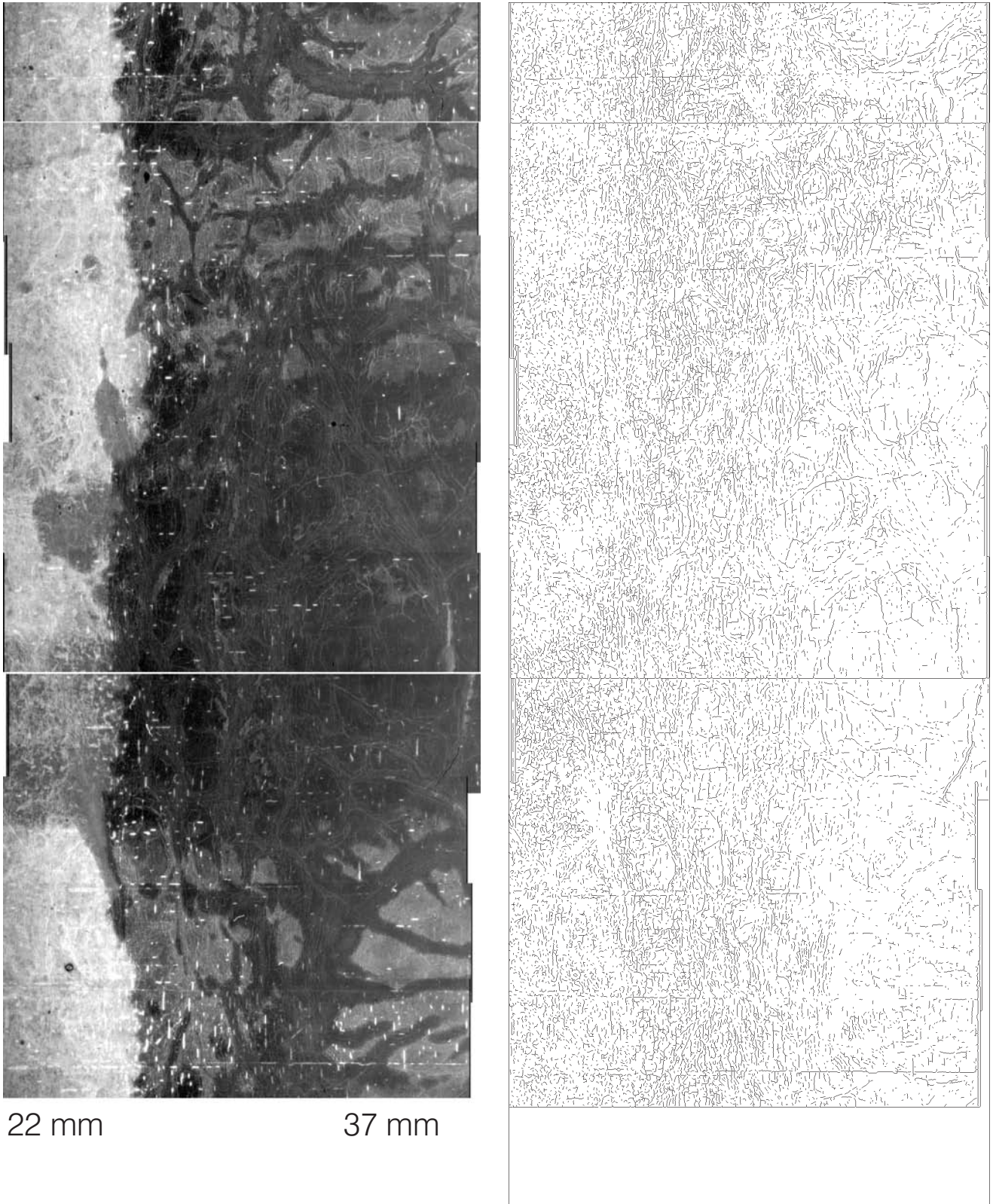
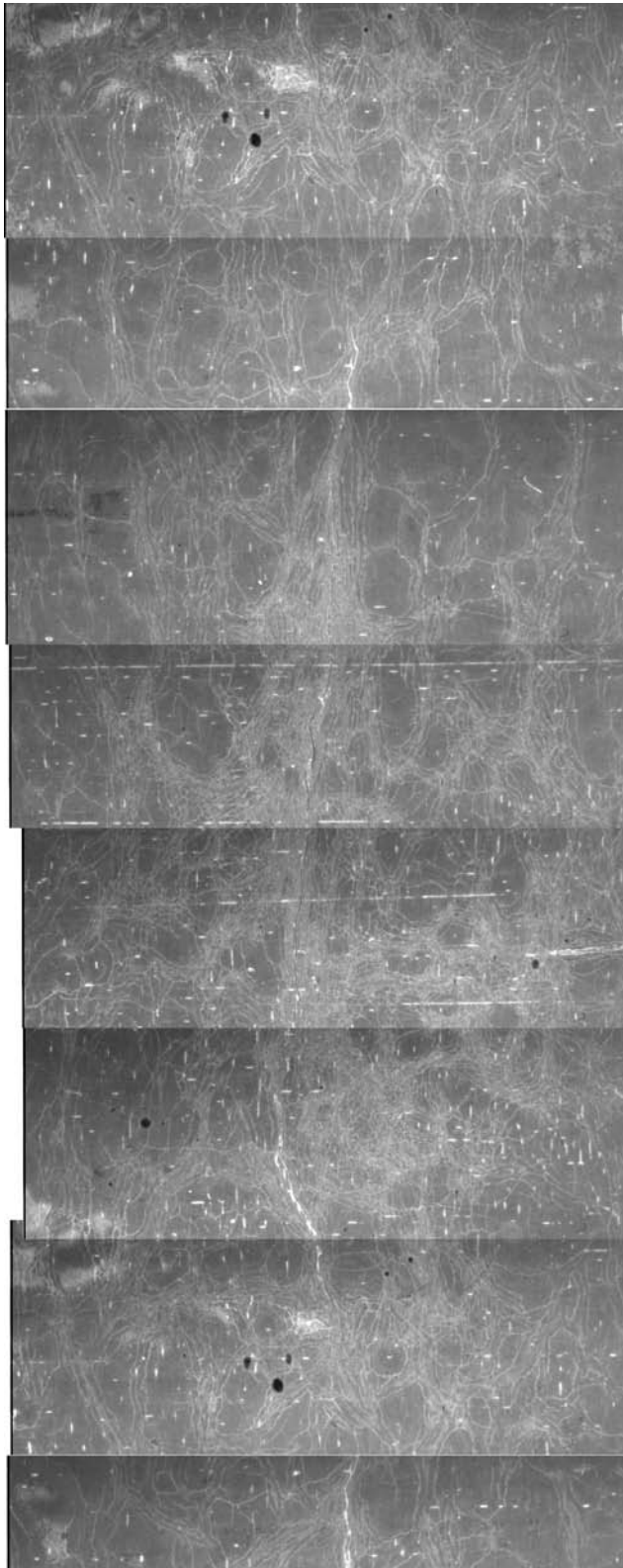


Fig. 21: experiment 19066 (1600°C, 300 μm oxide thickness)
left: circumference image between 22 and 37 mm
with solvent injection showing albedo decrease along cracks
right: lines extracted with hellgrat.mac



48 mm

63 mm

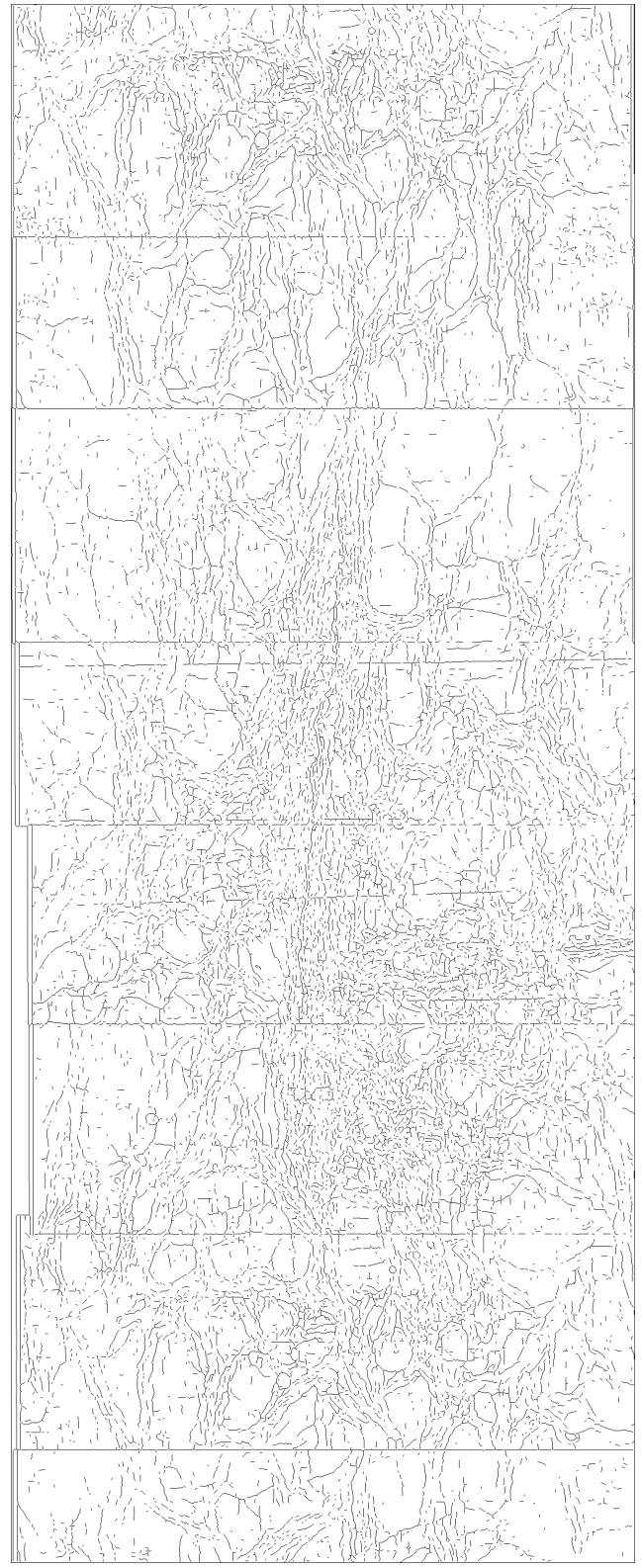


Fig. 22: experiment 19066 (1600°C, 300 μm oxide thickness)
left: circumference image between 48 and 63 mm
right: lines extracted with hellgrat.mac

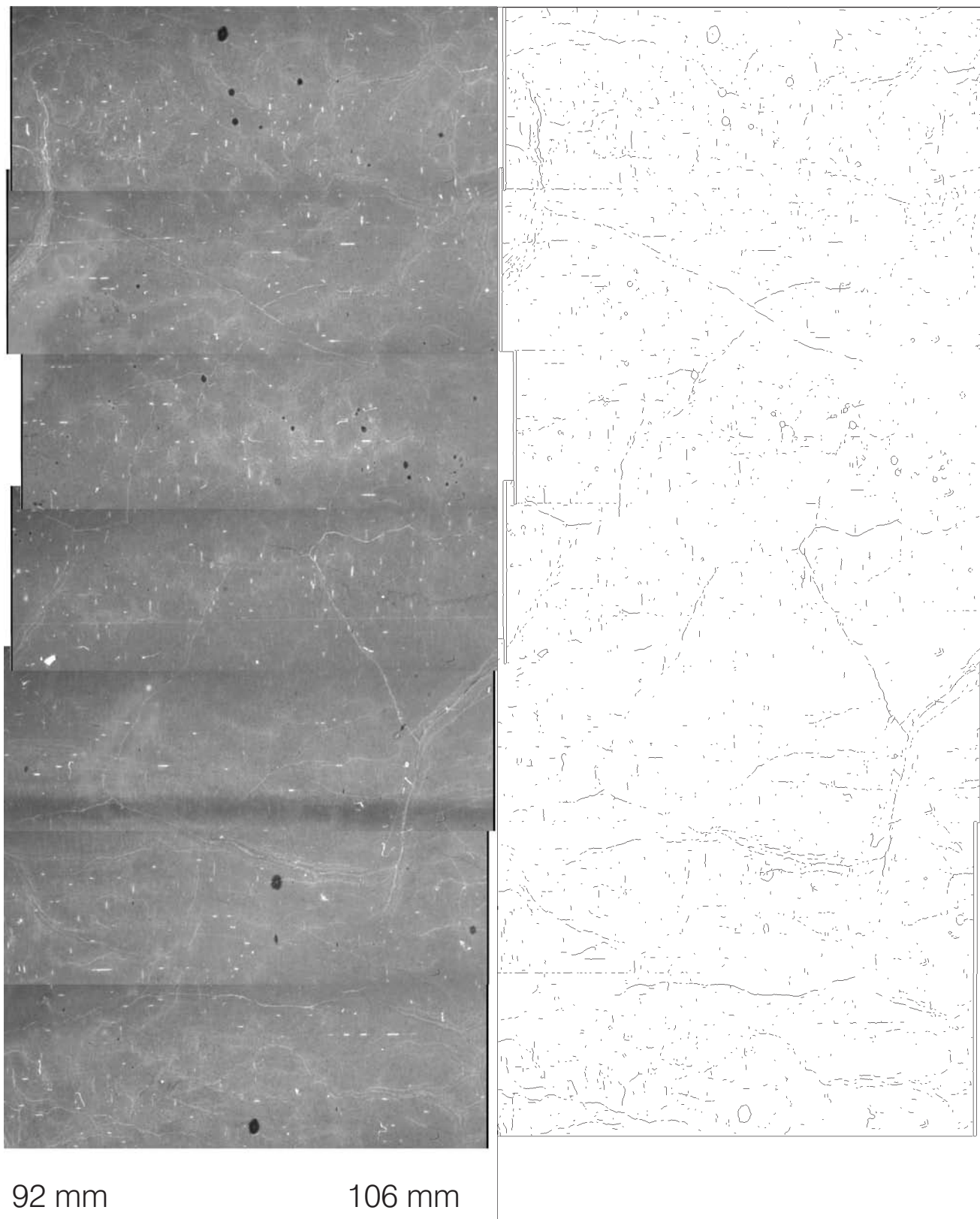
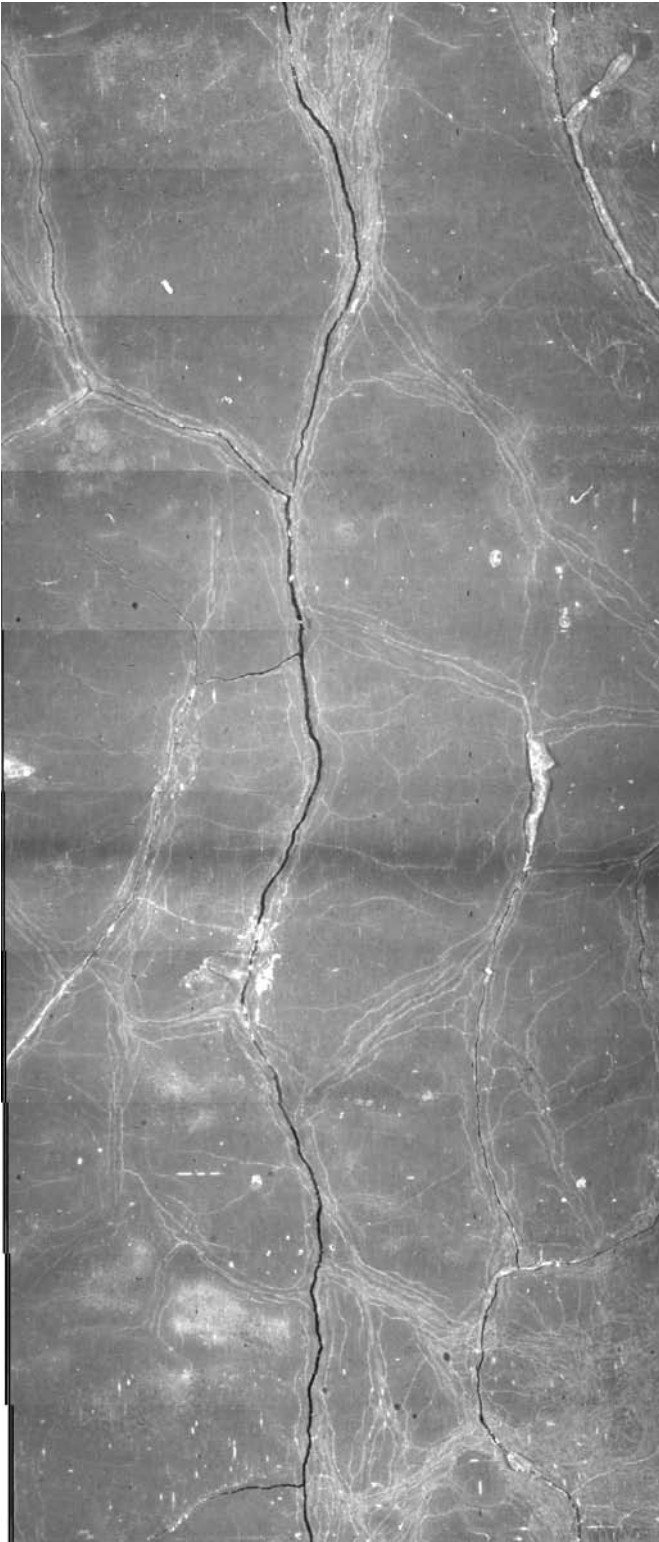


Fig. 23: experiment 19066 (1600°C, 300 μm oxide thickness)
left: circumference image between 92 and 106 mm
right: lines extracted with hellgrat.mac

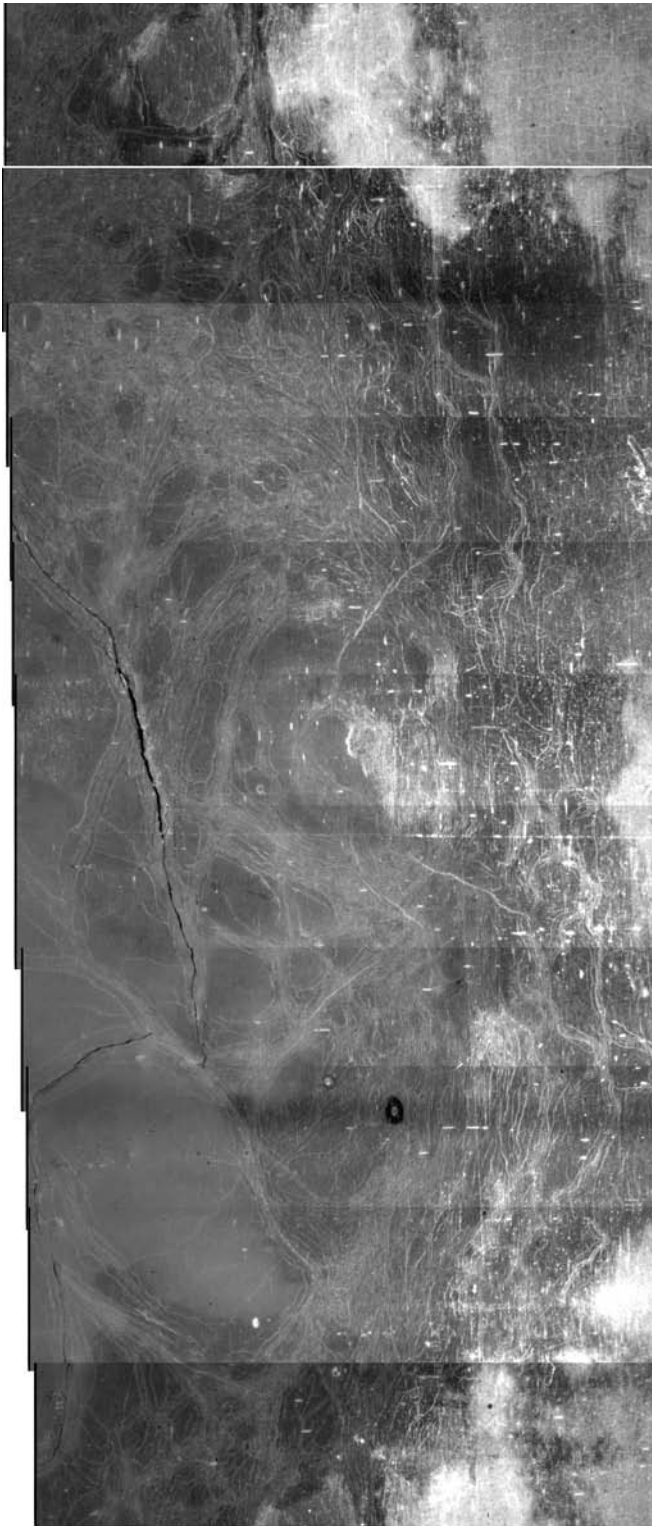


110 mm



124 mm

Fig. 24: experiment 19066 (1600°C, 300 μm oxide thickness)
left: circumference image between 110 and 124 mm
right: lines extracted with hellgrat.mac



128mm

145 mm

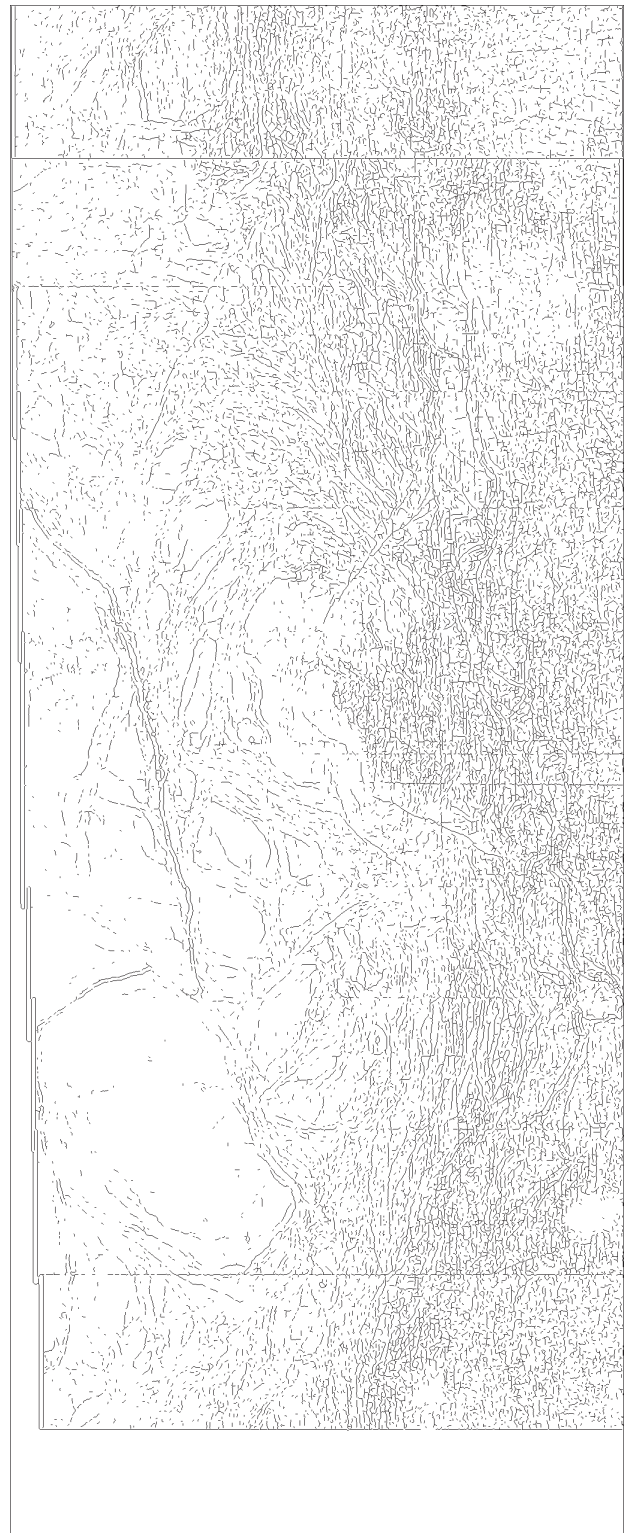


Fig. 25: experiment 19066 (1600°C, 300 μm oxide thickness)
left: circumference image between 128 and 145 mm
right: lines extracted with hellgrat.mac

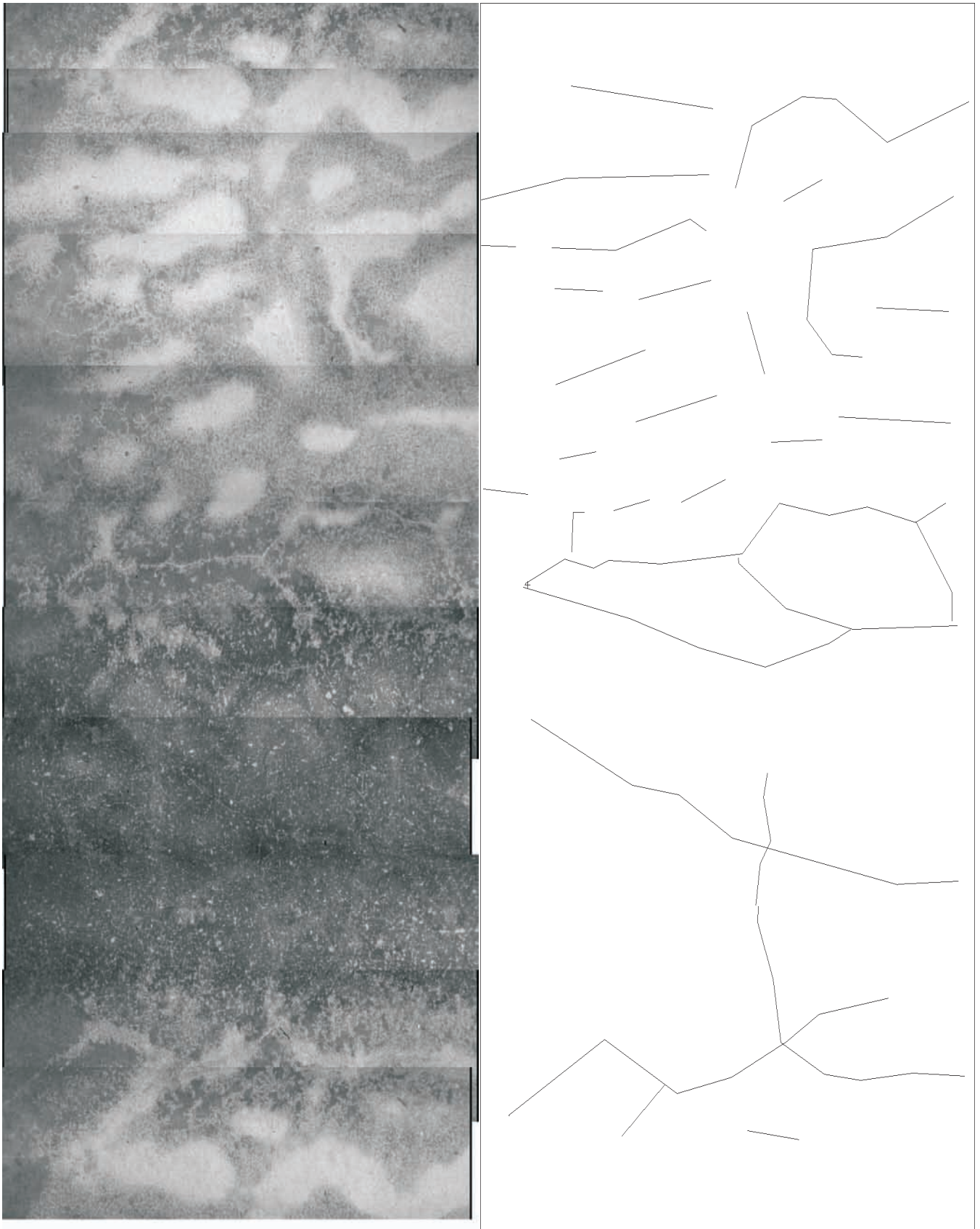


Fig. 26: experiment 05066 (1400 °C, 300 μm oxide thickness)
left: circumference between 55 and 71 mm after solvent injection,
right: hand tracing of crack lines with solvent bleeding

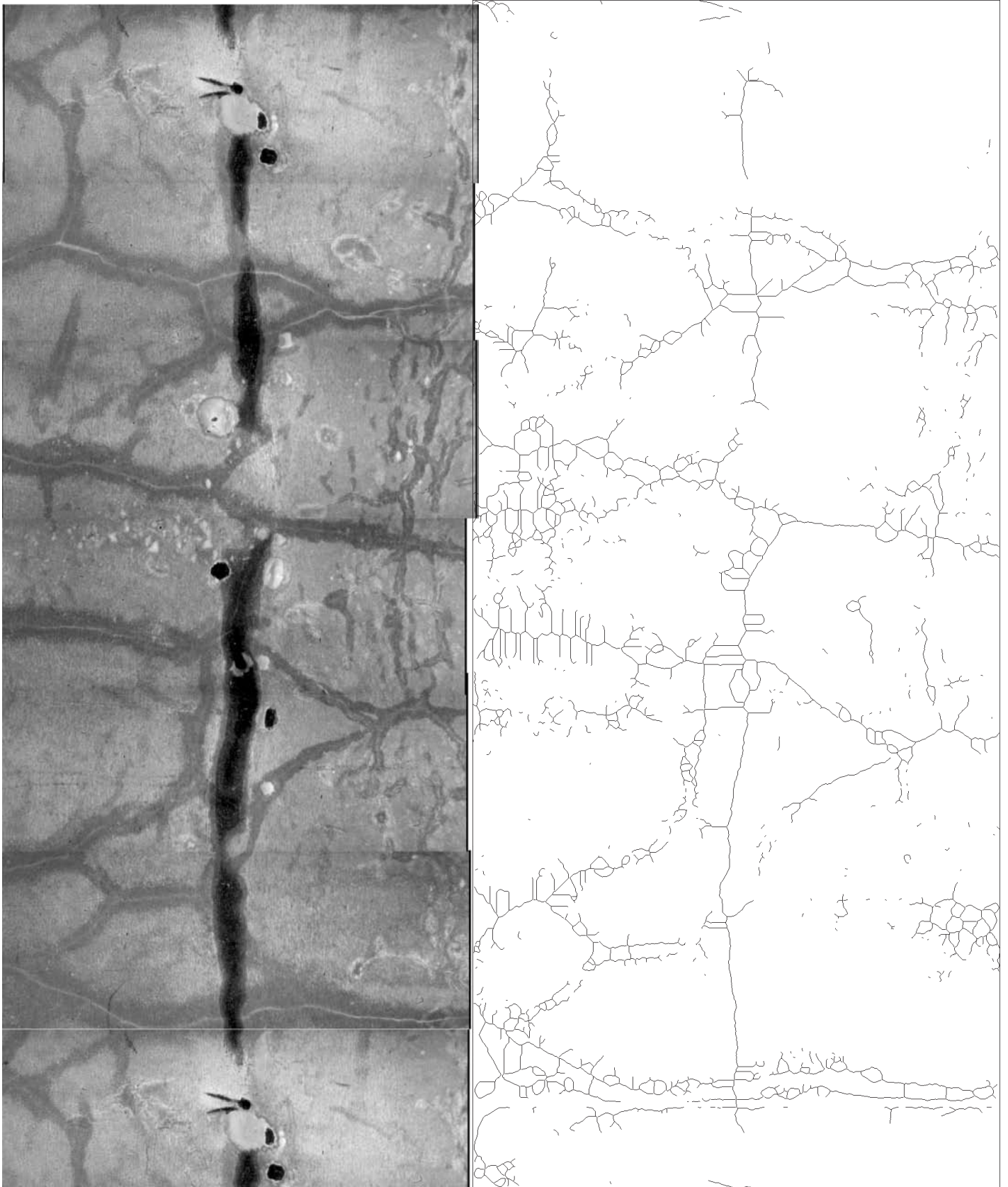
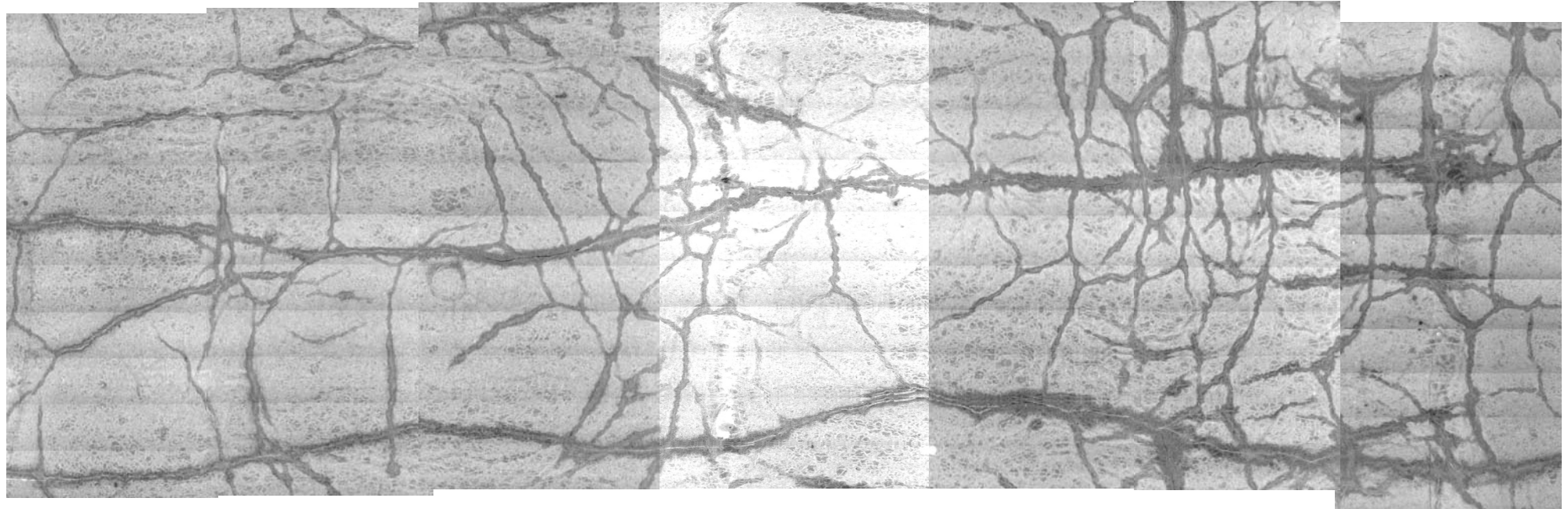


Fig.27 : experiment 27027 (1600°C, 300 μm)
left: circumference image at center TC location
right: crack grid according to acetone.mac,
total length: 456 mm

<--top

bottom-->



265 mm

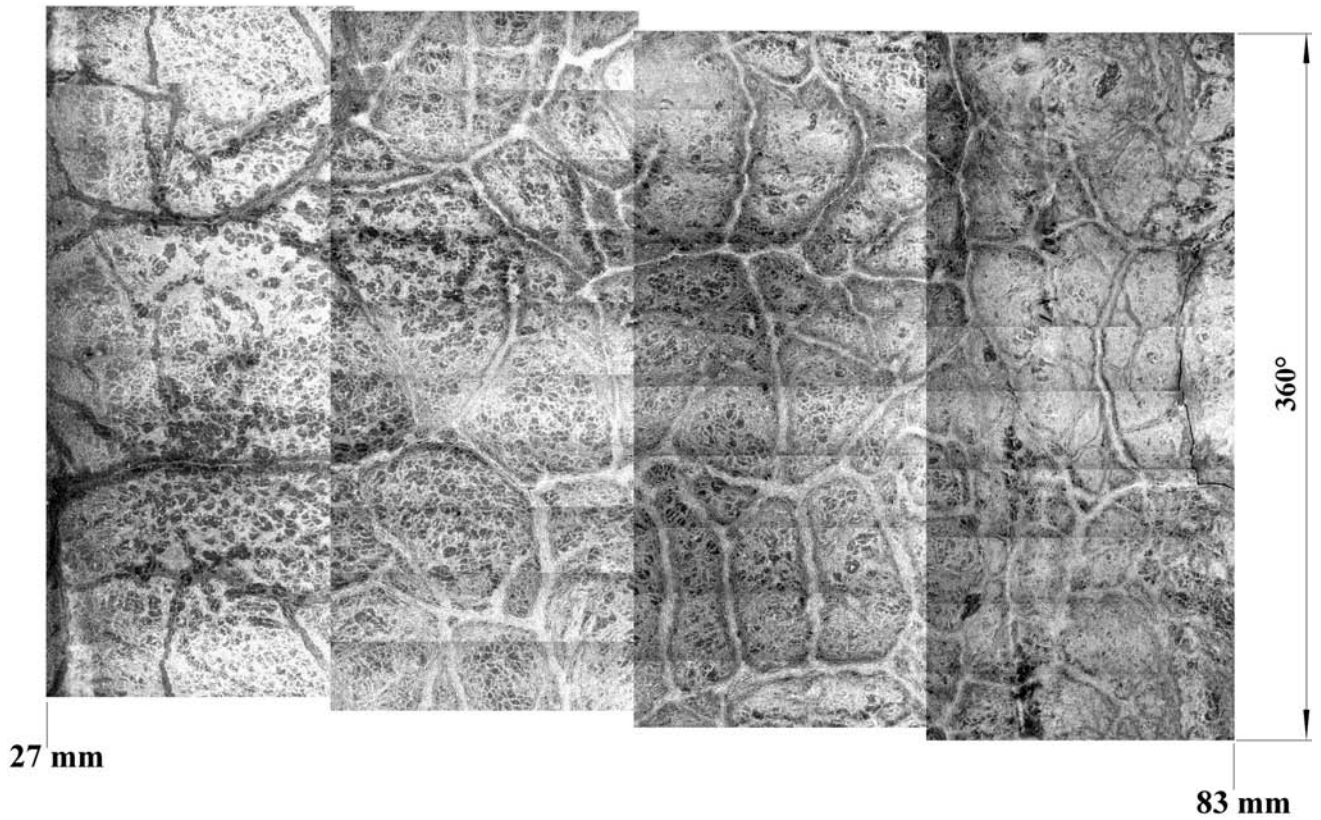
320mm

<crack lengths>

330mm

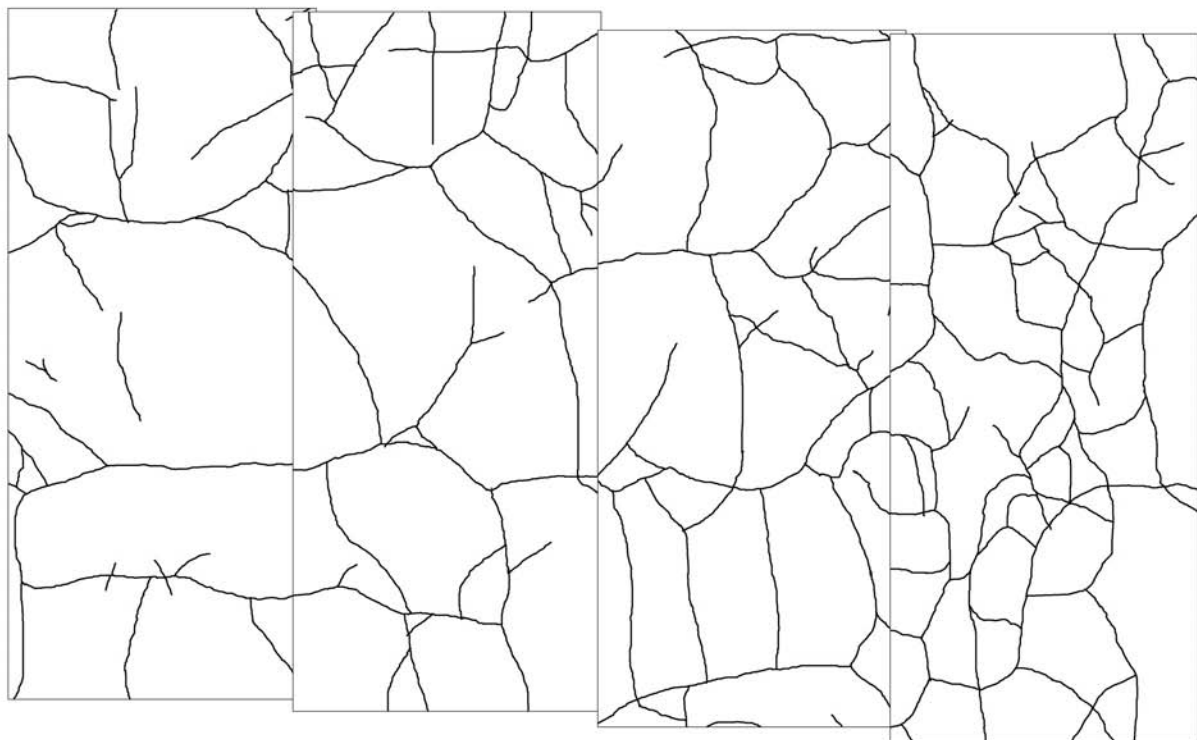
478mm

Fig. 28: surface of experiment 09047 (1200 °C, 250 μm oxide thickness) after solvent injection between 20 and 118 mm assembled from 70 subimages crack length calculation with acetone.mac in 4 subimages



27 mm

83 mm



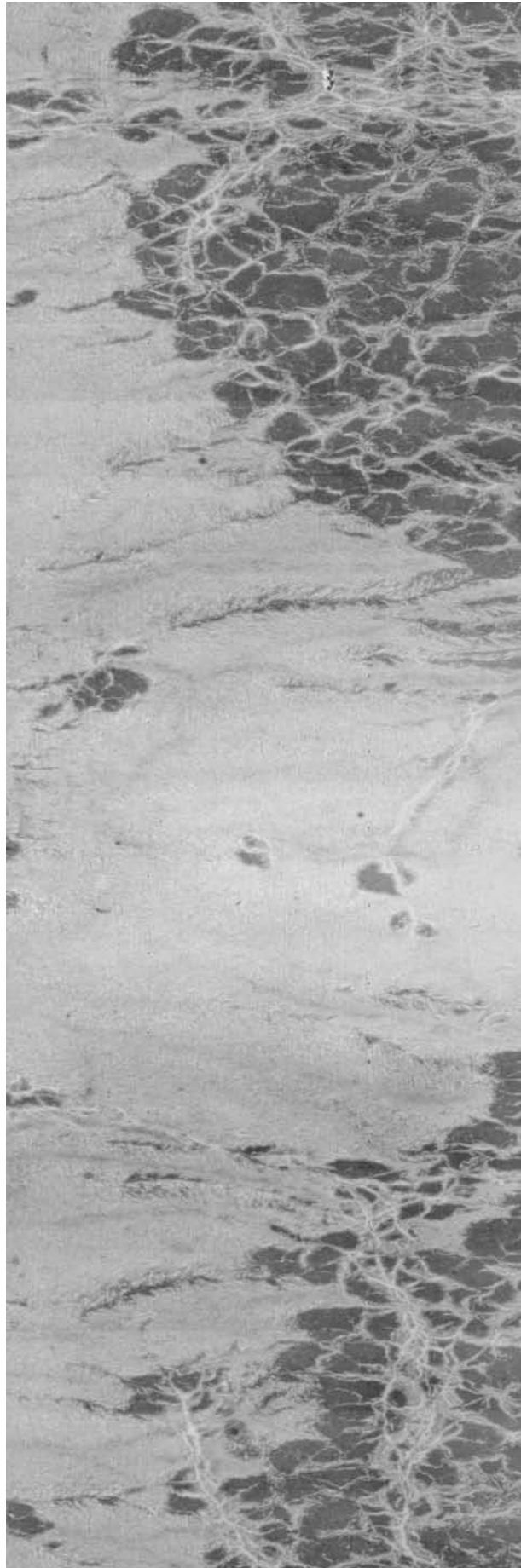
crack density:
 0.33 mm^{-1}

crack density:
 0.40 mm^{-1}

crack density:
 0.45 mm^{-1}

crack density:
 0.57 mm^{-1}

Fig.29: Sample 100471
(δ_{ZrO_2} =240 μm , $t_{\text{cool.}}$ =1200 $^{\circ}\text{C}$, steam flow rate 1.5 g/s)



black

areas:

180 μm

oxide

thickness

bright

area:

200-220

μm oxide

thickness

Fig. 30: experiment 11047 (1200°C, 200 μm)
circumference image
at begin of black stained area

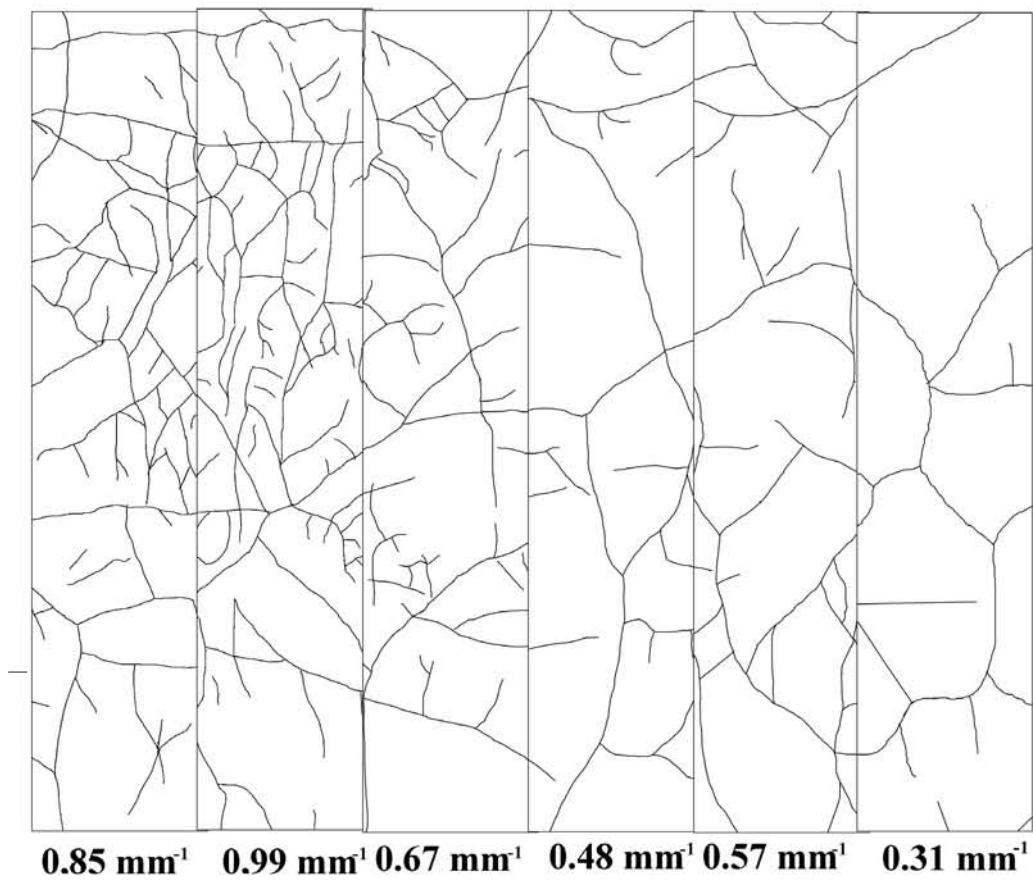
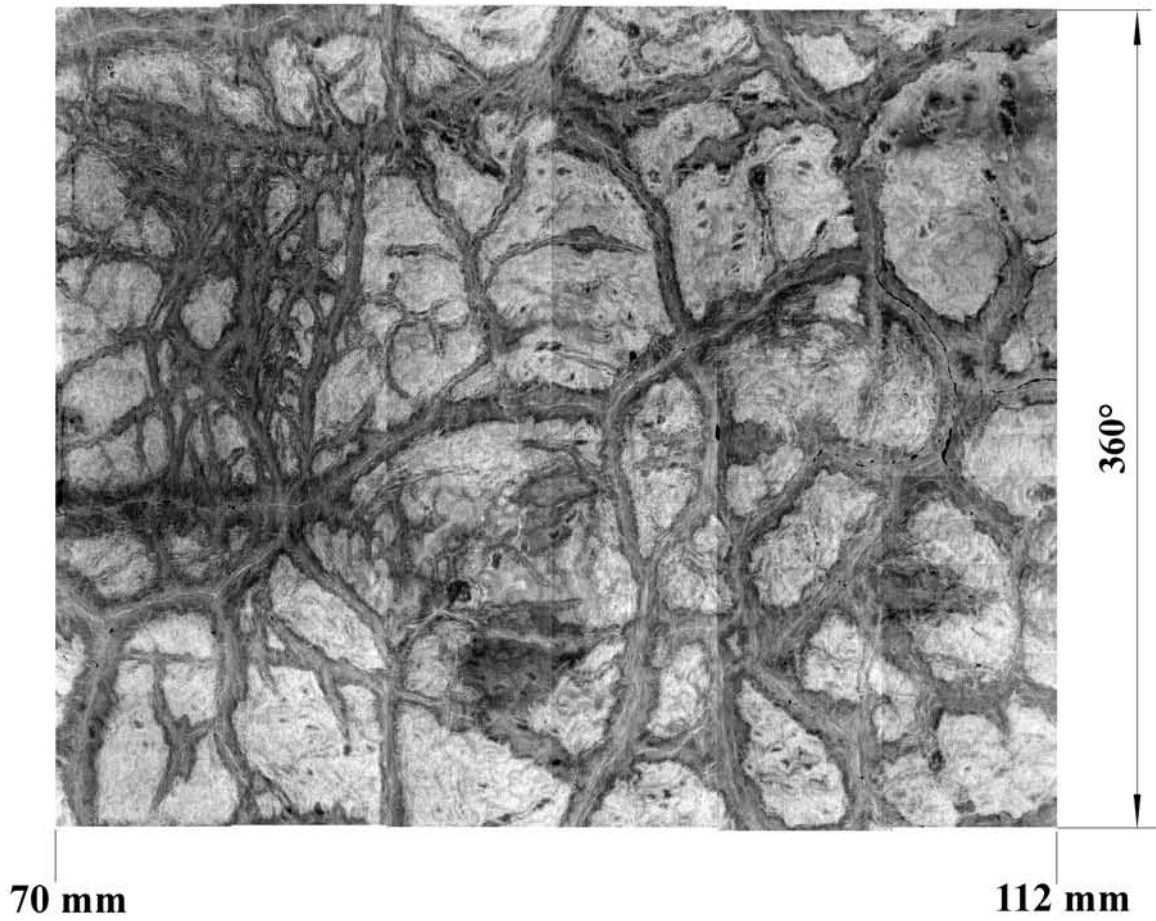


Fig. 31: Sample 200272, surface and crack pattern ($\delta_{\text{ZrO}_2}=260\mu\text{m}$, $t_{\text{cool.}}=1400^\circ\text{C}$, steam flow rate 0.08g/s)

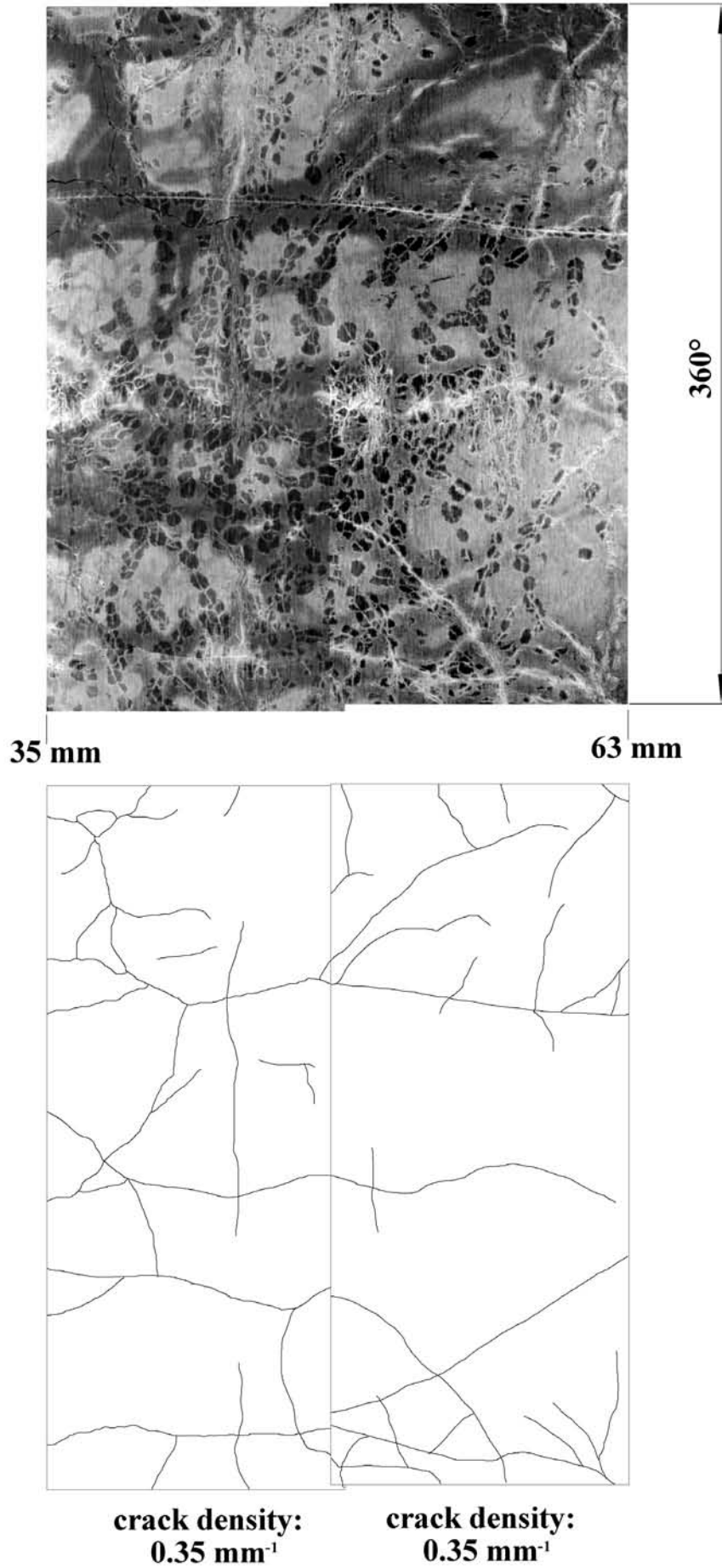


Fig. 32: Sample 040771, surface and crack pattern ($\delta_{ZrO_2}=290\mu\text{m}$, $t_{\text{cool.}}=1400^\circ\text{C}$, steam flow rate 1.5 g/s)

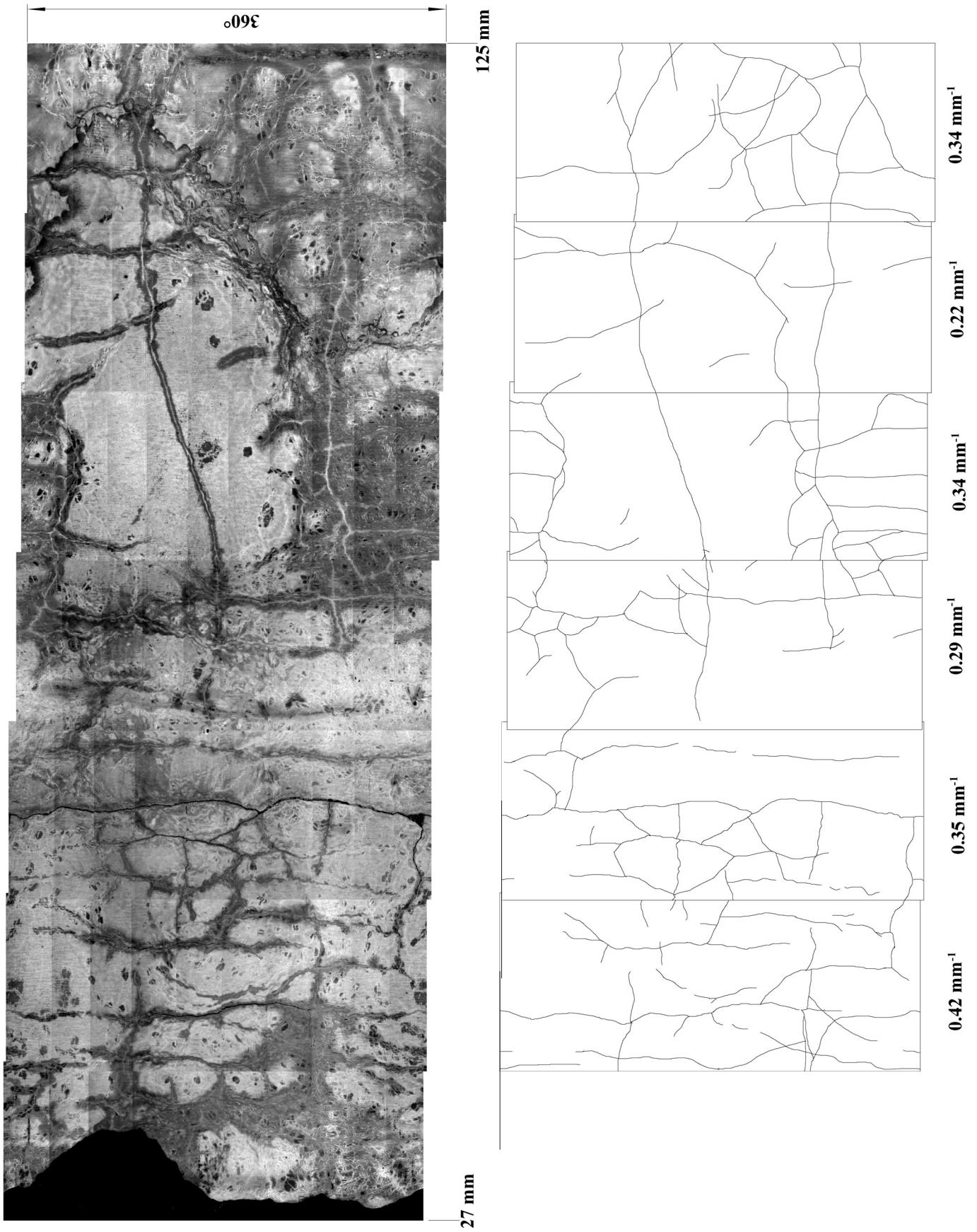


Fig. 33: Sample 080771
 $\delta_{\text{ZrO}_2} = 250 \mu\text{m}$, $t_{\text{cool.}} = 1400^\circ\text{C}$, steam flow rate
 (initiated 120s before cooldown starts) 1.5 g/s

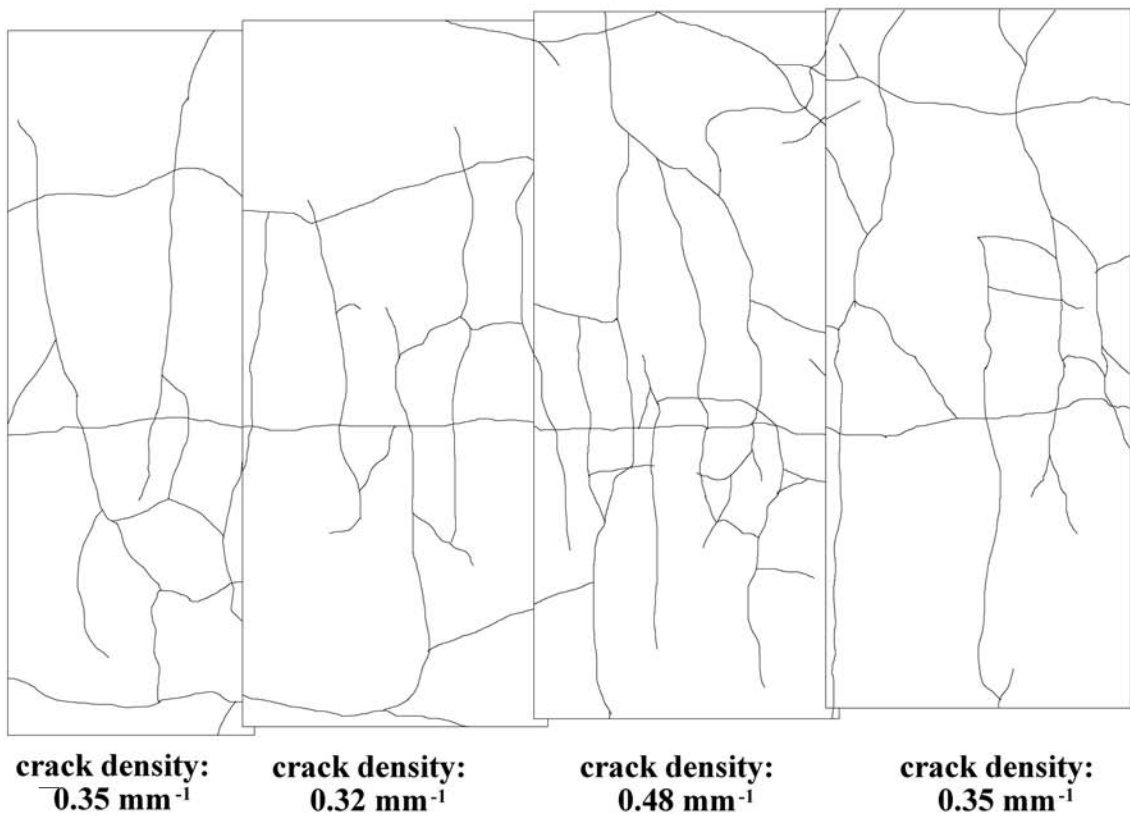
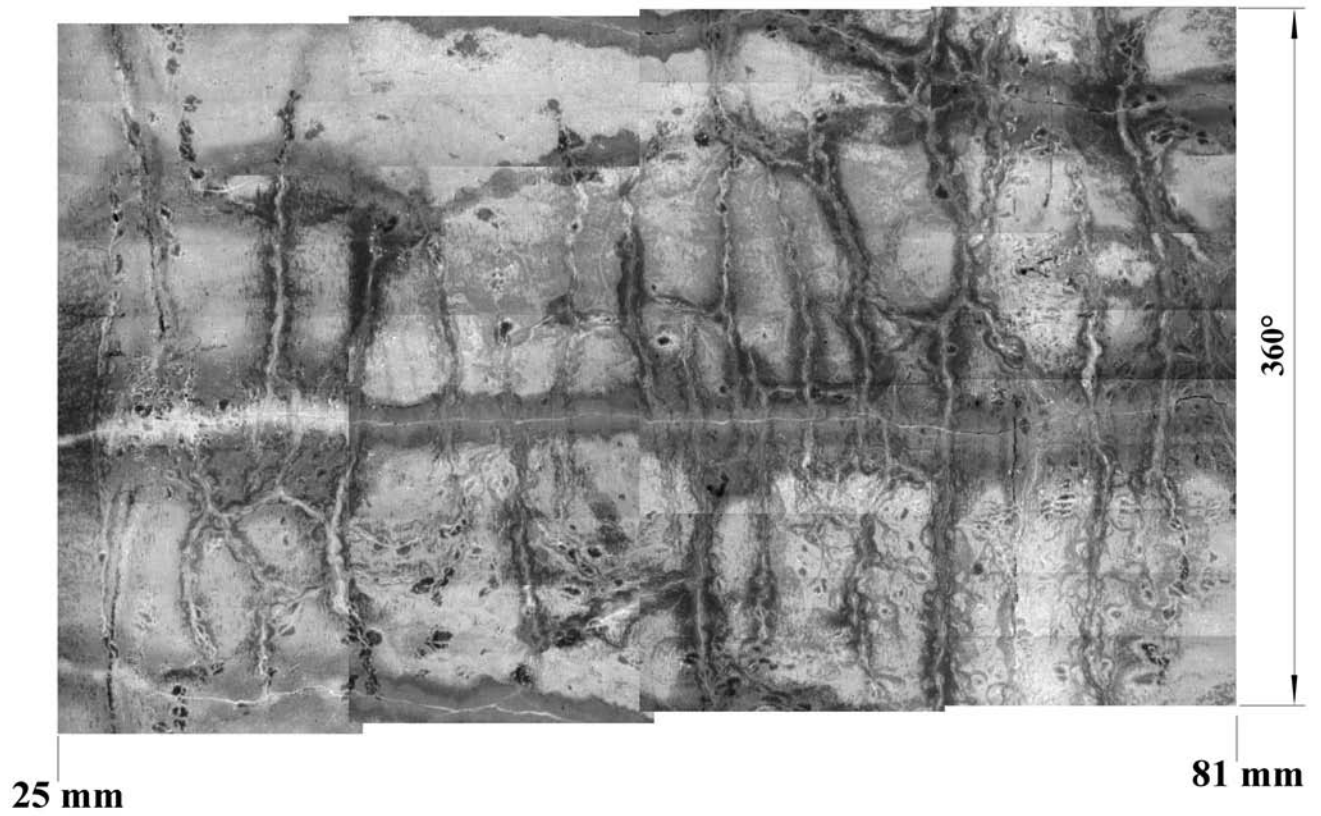


Fig. 34: Sample 080772 -lower part-
($\delta_{\text{ZrO}_2}=220\mu\text{m}$, $t_{\text{cool.}}=1400^\circ\text{C}$, steam flow rate 0.08 g/s)

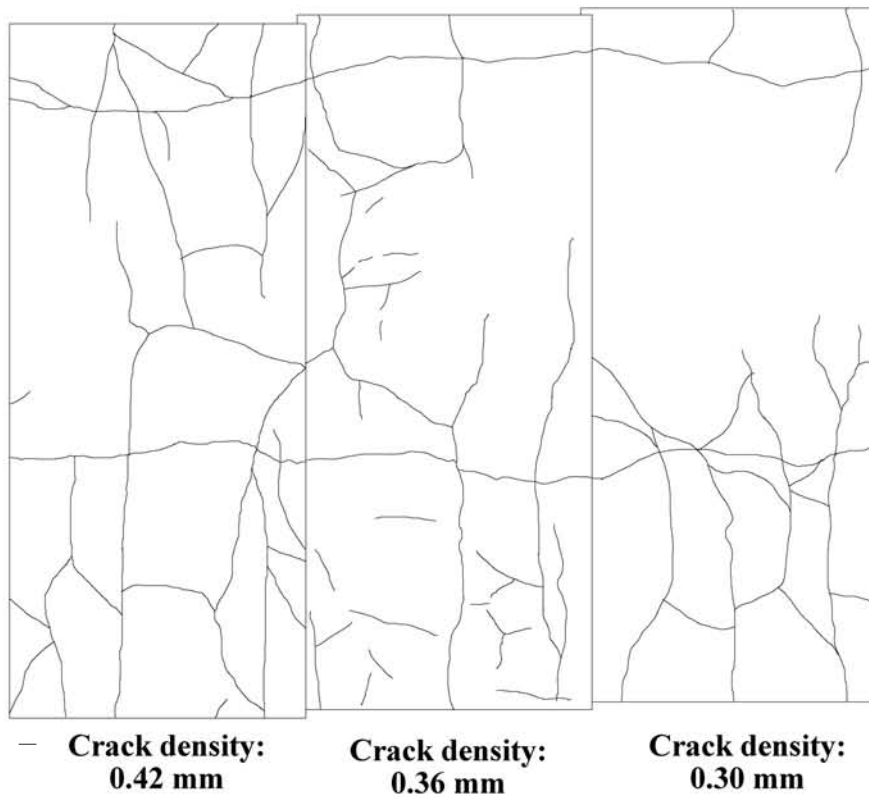
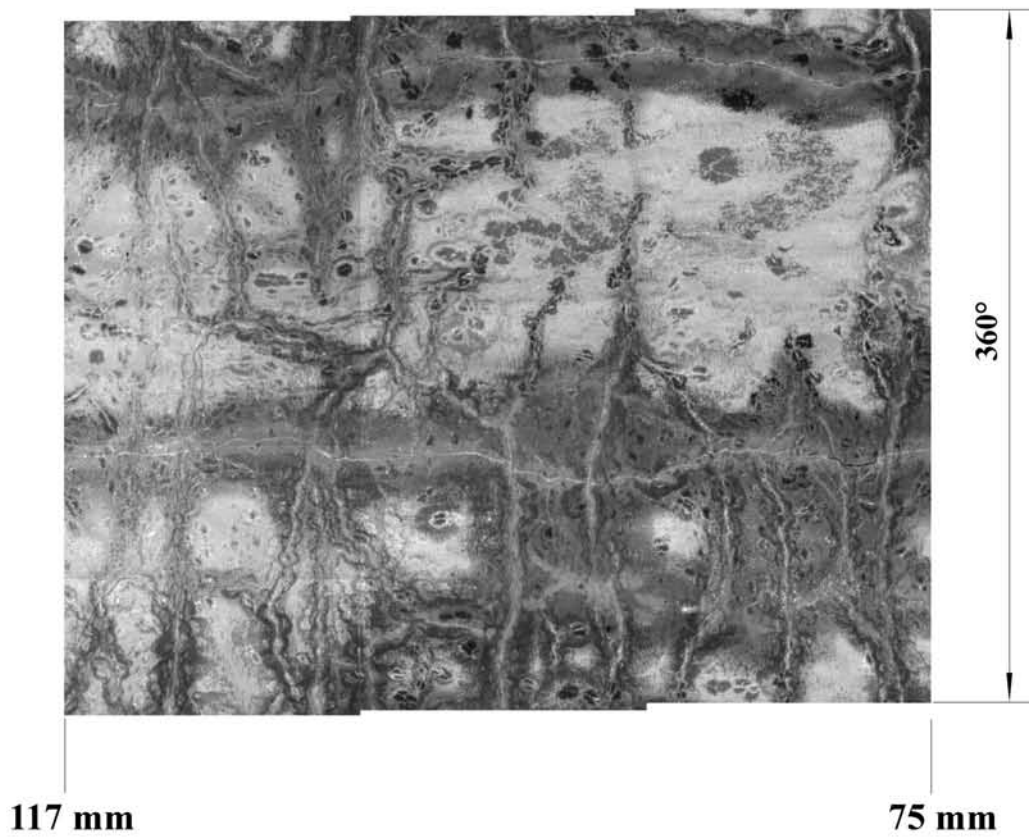


Fig. 35: Sample 080772 -upper part-
($\delta_{\text{ZrO}_2} = 220\mu\text{m}$, $t_{\text{cool.}} = 1400^\circ\text{C}$, steam flow rate 0.08 g/s)

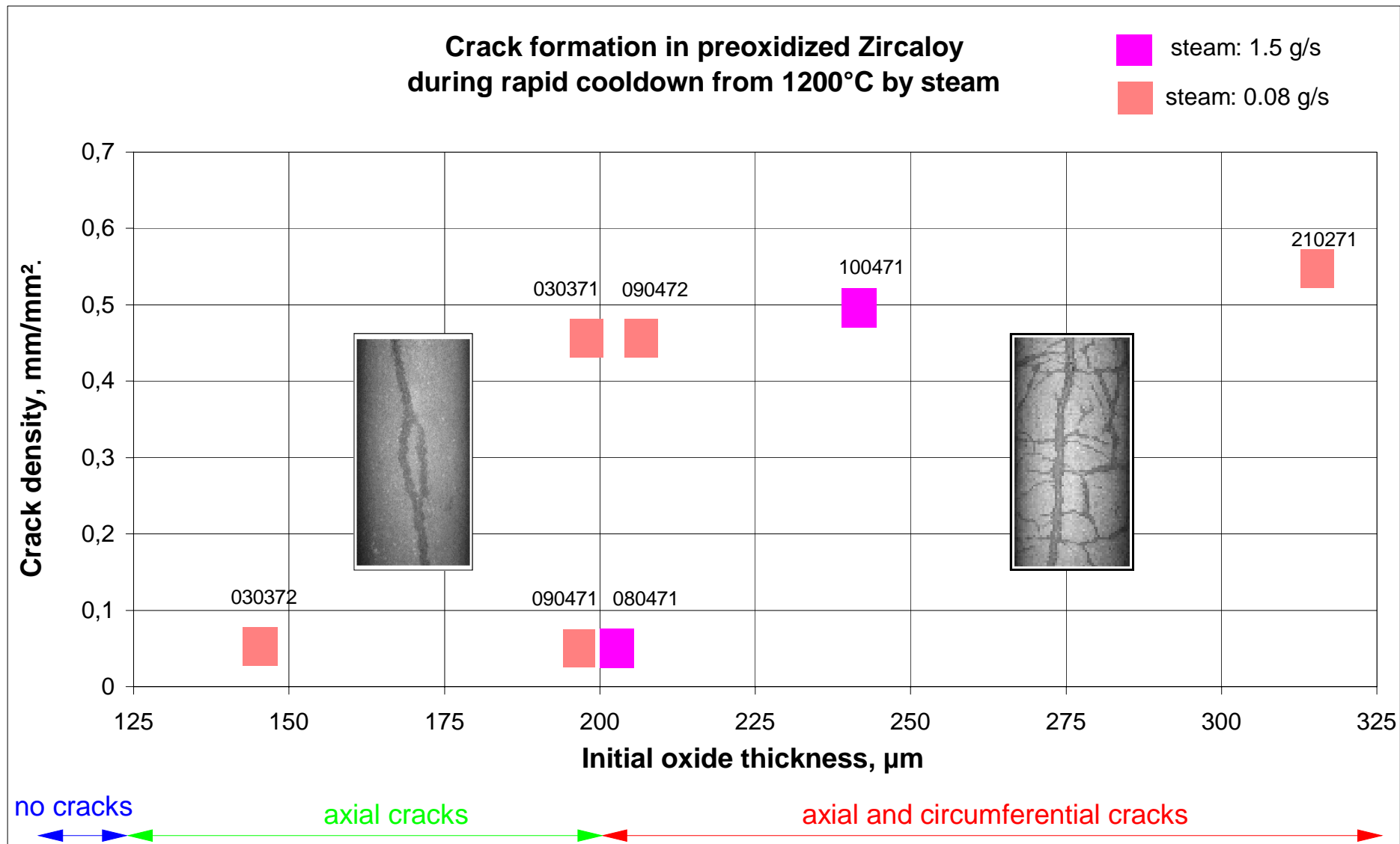


Fig.36. Dependence of the crack density from the oxide layer thickness by steam cooldown at 1200°C.

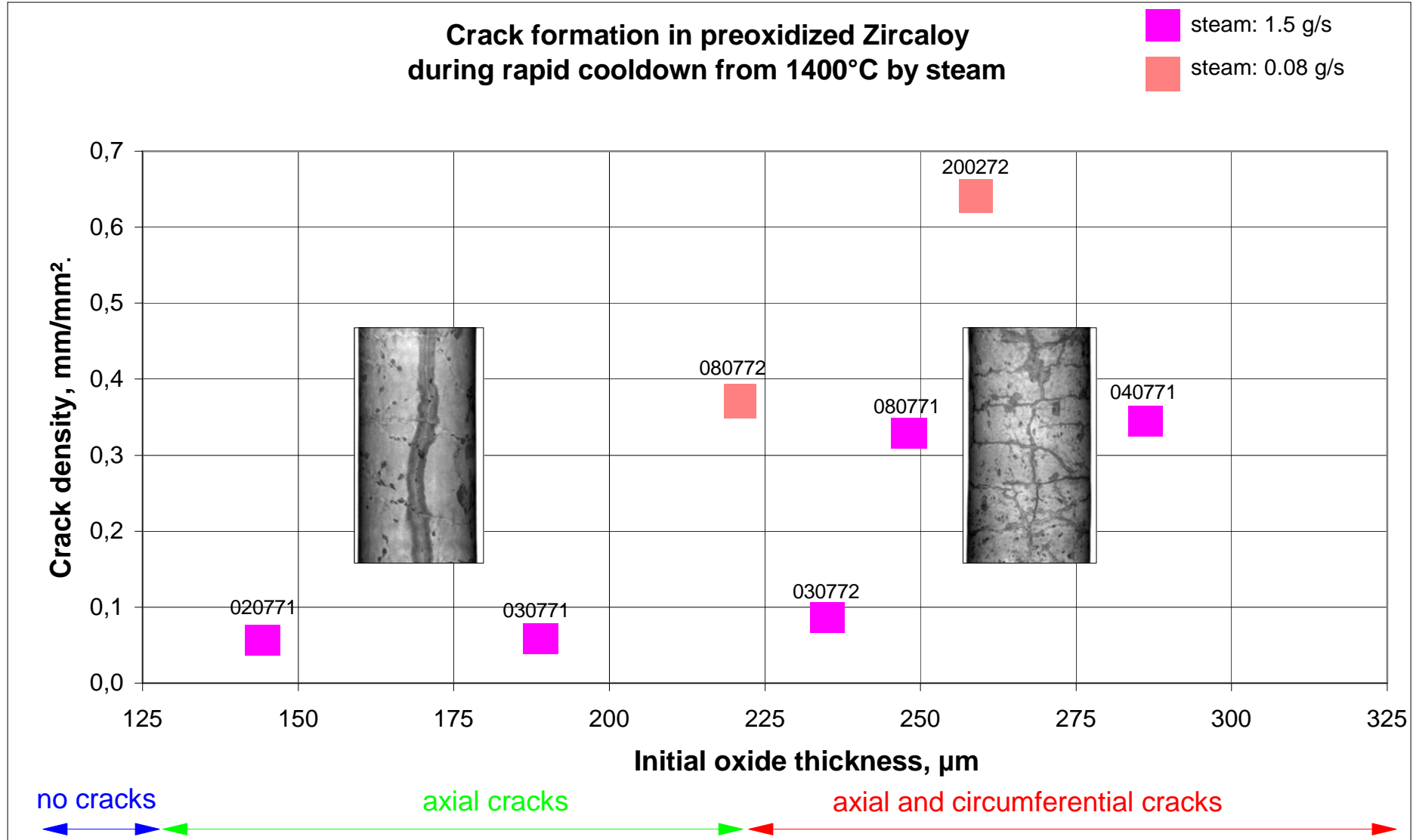


Fig.37. Dependence of the crack density from the oxide layer thickness by steam cooldown at 1400°C.